WAVELET TRANSFORMS FOR THE SIMULATION OF FLOW PROCESSES IN POROUS AND FRACTURED GEOLOGIC MEDIA

A Thesis

by

QIAOYIRU WANG

Submitted to the Graduate and Professional School of
Texas A&M University
in partial fulfillment of the requirements for the degree of

MASTER OF SCIENCE

Chair of Committee,	George J. Moridis
Co-Chair of Committee,	Thomas A. Blasingame
Committee Members,	Eduardo Gildin
	Yalchin Efendiev
Head of Department,	Jeff Spath

August 2021

Major Subject: Petroleum Engineering

ABSTRACT

Wavelets are localized small waves that exhibit the characteristic oscillatory behavior of waves with an amplitude that declines rapidly to zero. Their properties include orthogonality or biorthogonality, a natural multiresolution and, often, compact support. These properties can be used to repeatedly rescale a signal or a function, decomposing it to a desirable level, and obtaining and preserving trend and detail data at all scales that allow re-composition of the original signal.

The overall goal of this research is to create a set of wavelet-based (WB) numerical methods using different wavelet bases for application to the solution of the PDEs of interest to petroleum engineering. To address the problem, a new flow simulator WTFGS (Wavelet Transform Flow and Geomechanics Simulator) has been developed, which is written in MATLAB, where this code couples wavelet transform with a standard Finite-Difference scheme. In the current state of development, the WB numerical solution is verified against analytical solutions of 1D problems for liquid flow through porous media and is validated through comparisons to numerical solutions for problems of 2D and 3D flow through porous media obtained from a conventional numerical simulator.

DEDICATION

This work is dedicated to my father, my mother, and my grandparents who always give me unconditional and endless love and support.

ACKNOWLEDGEMENTS

First and foremost, I would like to express my sincere appreciation to my committee chair, Dr. George J. Moridis, for his support and guidance throughout this research project. Dr. Moridis' unwavering enthusiasm for scientific research inspired me throughout my academic and research students and has kept me consistently craving for knowledge. The insightful feedback of Dr. Moridis has pushed me to explore my potential and helped me to bring my work to a new level. I am eternally grateful for his supervision.

I would like to thank the co-chair of my committee, Dr. Thomas A. Blasingame, for his encouragement, dedication, and time to train me to be an academically professional student. The endeavor and perfectionism Dr. Blasingame requires of himself and his students always reminds me to give my absolute best effort.

I also would like to thank Dr. Eduardo Gildin for his excellent course, his kindness, and his patience which helped me to improve my programming abilities significantly, I began as a novice programmer and Dr. Gildin's patient guidance helped me to choose to focus my research on the field of numerical simulation.

Lastly, I would like to thank Dr. Yalchin Efendiev for serving as the external member of my advisory committee.

CONTRIBUTORS AND FUNDING SOURCES

Contributors

This work was supervised by a thesis committee consisting of Professor Moridis [advisor], Professor Blasingame [co-advisor], Professor Gildin of the Department of Petroleum Engineering, and Professor Efendiev of the Department of Mathematics.

Funding Sources

This graduate study was supported by a research assistantship from the Texas Engineering Experiment Station and the Department of Petroleum Engineering at Texas A&M University, both parts of the start-up funding of the projects of Dr. George Moridis.

The contents of the work are solely the responsibility of the student and her advisory committee, and do not necessarily represent the official views of the funding sources cited above.

NOMENCLATURE

Variables:

A	=	cross-section area, m^2
a	=	wavelet expansion coefficients
B	=	formation volume factor, bbl/STB
c_t	=	total compressibility, Pa^{-1}
f	=	a general function
g	=	gravitational acceleration, (= 9.806) m/s^2
h	=	Haar wavelet family
I	=	an integral of a Haar wavelet
J	=	maximum level of resolution
j	=	scaling factor
k	=	translation factor
k_f	=	intrinsic permeability, m^2
$\overrightarrow{k_f}$	=	permeability tensor, m^2
L	=	Lebesque integral
L^2	=	square-integrable function
L_2	=	error norm
L_∞	=	error norm
l^2	=	square-integrable sequence

$\mathcal{L}\{\ \}$	=	Laplace transform of the quantity within the brackets
m	=	defined in Eq. (4.2.5)
m	=	production flux, kg/s/m^3
N_m	=	B-spline of order m
p	=	pressure, Pa
q	=	production rate, kg/s
$\tilde{q}_{sc}$	=	strength of the source of sink, sec^{-1}
$\mathbb{R}$	=	the set of real numbers
s	=	time step number
t	=	time, sec
t_{st}	=	starting point in time
t_{end}	=	ending point in time
Δt	=	time subinterval
x	=	Cartesian coordinates, m
Δx	=	x domain subinterval
x_e	=	total length of x domain, m
y	=	Cartesian coordinates, m
y_e	=	total length of y domain, m
z	=	Cartesian coordinates, m
z_e	=	total length of z domain, m
z_g	=	elevation

$\mathbb{Z}$ = the set of integers

Greek Symbols:

ε = absolute error

η = relative error

ξ = subdomain

λ = mobility, $m^2/(Pa \cdot s)$

μ = fluid viscosity, Pa·s

ρ = fluid density, kg/m^3

Φ = multidimensional wavelet scaling function

ϕ = porosity, fraction

φ = wavelet scaling function

Ψ = multidimensional wavelet

ψ = mother wavelet

Ω = a general bounded domain

ζ = domain

Subscripts and Superscripts:

D = dimensionless

i = i-th wavelet

j = scaling factor of wavelet

k = translation factor of wavelet

m	=	the order of B-spline
SC	=	standard condition

Acronyms and Abbreviations:

BEM	=	Boundary Element Method
BSWL	=	B-spline Wavelet on the Interval
DAF	=	Distributed Approximating Functional
FDM	=	Finite Difference Method
FEM	=	Finite Element Method
FFT	=	Fast Fourier Transform
HCSWI	=	Hermit Cubic Spline Wavelet on the Interval
MRA	=	Multiresolution Analysis
PDE	=	Partial Differential Equation
ULP	=	Ultra-Low Permeability
WB	=	Wavelet-Based
WGM	=	Wavelet-Galerkin Method
WCM	=	Wavelet-Collocation Method
WTFGS	=	Wavelet Transform Flow and Geomechanics Simulator

TABLE OF CONTENTS

Page

LIST OF FIGURES

Page

LIST OF TABLES

Page

CHAPTER I

INTRODUCTION AND LITERATURE REVIEW

1.1 Background

The first wavelet was introduced by Haar (1910). The basic concept of wavelet analysis, *i.e.*, translation, dilation and trade-off between time and frequency resolution, was proposed in the early 1980's (Morlet, 1982; Grossman and Morlet, 1984). However, it was not until the development of orthogonal bases of compactly supported wavelets (Daubechies, 1988, 1990, 1992) and the algorithm for multiresolution analysis (Mallat, 1989) that the subject of wavelet analysis caught the attention of both mathematicians and engineers in signal processing, image processing, and numerical analysis.

Wavelets are defined as oscillating functions of time or space with an amplitude that rapidly declines to zero. Some researchers view wavelets as a modern tool for solving time-frequency problems because of their ability to analyze non-stationary, transient, and time-varying behaviors. Some in applied mathematics communities consider wavelets a new topic because of their rapid development. Others treat it as a new basis to represent functions.

Wavelets were first noted as an effective tool in signal and image compressing because these functions enable most signals and images to be decomposed as sparse multiscale representations by wavelet bases. In other words, many wavelet- associated coefficients are zero or at least very small, so they can be neglected and reduce the related complexity

and computational burden. Moreover, wavelets allow control of the estimated error by controlling the terms of neglected coefficients that can cause errors.

Besides compression, the multiscale representation of wavelets allows the detection of edges or textures in an image, an attribute that has been used in the FBI's Fingerprint Identification System (Bradley, 1993). This system created a database of fingerprints using a sparse format which requires the storage of only a few parameters and resulted in a vastly more efficient identification. Wavelets are also very effective in de-noising, which is used in the transformation of different music formats.

Because of the success of wavelet techniques in the areas mentioned above, scientists proposed the use of wavelet methods for the solution of partial differential equations (PDEs). In particular, the compression properties of wavelets could represent solution domains that have localized features. However, the expectations of using wavelet methods to solve PDEs were not quickly met with success or wide acceptance. One reason is that PDEs are defined on general bounded domains instead of an interval or a square domain of signals and images. Another reason is that the compression and error control properties of wavelets rely on a mathematical framework that needs to be extended to the bounded domain for differential equations. In order to solve the problems mentioned above, researchers in wavelet numerical methods have made significant progress (Chui and Wang, 1991, 1992a, 1992b, 1993) which, however, lags behind the success of wavelet application to other disciplines of science and engineering.

For numerical analysis, a function in $L^2(\mathbb{R})$ can be decomposed into, and reconstructed by, its wavelet bases. Wavelets often have three important properties: orthogonality, multiresolution, and compact support. The orthogonality (or semi-orthogonality) property can simplify computations. The multiresolution analysis (MRA) properties can be used to form multiscale wavelet bases, and the compact support guarantees that the function is nonzero only on a finite interval. Because of the aforementioned properties, wavelets have been used in the solution of PDEs.

1.2 Application of Wavelets to the Solution of PDEs

During the past two decades, wavelet numerical methods using a variety of approaches have been developed for the solution of PDEs: (a) hybrid with weighted residual methods; (b) hybrid with finite element methods; and (c) hybrid with boundary element methods.

1.2.1 Wavelet-Weighted Residual Method

In the wavelet-weighted residual method, the wavelet functions or their scaling functions are used as weight functions in the solution domain. Wavelets (a) can represent functions at different resolution levels, and (b) are localized in space, which can allow local refinement within desired regions. The wavelet-weighted residual method mainly consists of two sub-methods (Li and Chen, 2014): the wavelet-Galerkin method (WGM) and the wavelet-collocation method (WCM).

In their application of WGM, Qian and Weiss (1993) used the Daubechies wavelet scaling functions as weight functions to solve the biharmonic Helmholtz equation in non-separable domains. Amaratunga and Williams (1994) used WCM to solve the two-

dimensional Poisson's equation with periodic boundary conditions. Then, by using the capacitance matrix method (Proskurowski and Widlund, 1976; O'Leary and Widlund, 1979), Dirichlet boundary conditions were imposed. WGM was found to converge much faster than the finite difference method and to have significant potential in developing hierarchical solutions. However, the capacitance matrix approach used in WGM with classic wavelet bases can result in a large residual error, and it additionally involves a complex construction procedure. To deal with these difficulties, Lu and Ohyoshi (1997) introduced a treatment in the one-dimensional wavelet-Galerkin system that replaced the boundary condition equations with end-equations.

Subsequently, Nakagoshi and Noguchi (2001) and Kim and Jang (2001) proposed a new adaptive WGM to analyze the Mindlin plates problem and the thin-walled box beam problem using interpolation wavelet functions. Ho and Yang (2001) used WGM to solve parabolic PDEs through the development of discretization formulations. Park and Tsiotras (2003) developed a successive wavelet-Galerkin projection scheme for solving the Hamilton-Jacobi Bellman equations. Al-Qassab and Nair (2003, 2004) used antiderivative wavelet bases as weight functions to solve the problem of free vibrations of an elastic cable.

The WGM exhibited its superiority in many engineering fields. Dahmen *et al.* (1995) investigated WGM for the solution of the Stokes equations. Yang *et al.* (1998) introduced WGM for computations in electromagnetic fields, especially for computing the associated connection coefficients. Venini and Morana (2001) used WGM for the solution of the one-dimensional elastic-plastic-damage constitutive model. Bindal *et al.*. (2003) proposed a

wavelet-Galerkin algorithm to solve the convection-diffusion problem. Wang and Pan (2004) used WGM for a phase field model describing microstructural evolution.

The applications of WGM over the past two decades exploited the multiresolution and localization properties of wavelets. Although this method has some drawbacks in dealing with the complexities of different types of boundary conditions, WGM is still attracting the attention of researchers, especially because of the capability of adaptive WGM to formulate functions on various levels of detail.

Similarly, WCM used wavelet functions as weight functions. McWilliam *et al.* (2000) used the Shannon wavelet functions to solve the stationary Fokker-Planck-Kolmogorov (FPK) equations, developed the n-dimensional solution method, and investigated the relationship between WCM and the Distributed Approximating Functional (DAF) approach. Chiavassa and Liandrat (2001) developed a fully adaptive wavelet-collocation algorithm to solve parabolic PDEs based on convolution operators. Cruz *et al.* (2001) introduced adaptive WCM to the chemical engineering community; they showed that this method was able to dynamically change the level of resolution, but also admitted that the adaptive WCM still needed further optimization.

Later, Park and Tsiotras (2003) developed a successive wavelet-collocation algorithm for approximations to optimal feedback control. Zhang *et al.* (2008) used WCM to convert differential equations into a set of algebraic equations that could easily handle the nonlinear terms. Vasilyev *et al.* (2000, 2005) developed an adaptive multilevel WCM for PDEs using second generation wavelets, namely lifted interpolating wavelets on an

interval. This numerical method was used for solving multidimensional elliptic problems constructed by the union of irregular grids. In addition, Zhou *et al.* (2008) developed a modified WCM to simulate the nonlinear vibration of multi-degree of freedom (MDOF) systems and achieved satisfactory accuracy.

Comparative studies between WGM and WCM were also conducted by many scholars. Vasilyev and Paolucci (1996) showed that the wavelet Galerkin approach mainly solves for the wavelet coefficients; the wavelet collocation approach provides solutions of the unknown function themselves at the collocation points. Nikolaou and Yong (1994) compared the Laplace-transform-wavelet-Galerkin method and the Laplace-transform-wavelet-collocation method in the solution of parabolic equations. Their results show that the latter method gives better approximation for parabolic equations. Further, Moridis *et al.* (1996) applied both WGM and WCM in solving two-phase flow problem through porous media using both Daubechies and Chui-Wang wavelet bases. Moridis *et al.* also concluded that the wavelet-collocation method is superior to the wavelet-Galerkin method under the conditions of that study.

Undoubtedly, even though the weighted residual method is a rather old method, the development of wavelets in the field of numerical analysis has revived this approach. Not only were the WGM and the WCM further developed over the past two decades, but scholars also proposed new variants such as the wavelet Petrov-Galerkin method (Chen *et al.*, 1997; Kaneko *et al.*, 2003) and the wavelet least squares method (Dahmen, 1985).

1.2.2 Wavelet-Finite Element Method

The finite element method (FEM) is a traditional and well-known method in the field of numerical analysis. Wavelets have been introduced as the trial functions of FEM. The wavelet-FEM can be categorized by the different wavelet bases it employs: the Daubechies wavelet; the spline wavelet; and the second-generation wavelet.

The Daubechies wavelet-FEM was first developed by Ko and Kurdila (1995), who showed the well-suited characteristics of this method for integral operator compression. The wavelet-FEM can solve the periodized PDEs in unbounded domains and both Dirichlet and Neumann boundary value problems on a specific class of bounded domains. Patton and Marks (1996) used a Daubechies scaling function as the interpolation function to develop a one-dimensional (1D) finite element. This element was used in dynamic test cases and the results showed reductions in both degrees of freedom and computational time.

Ma and Xue *et al.* (2003) also used the Daubechies scaling function to construct the wavelet-based beam element for the solution of beam bending problems. Chen and Yang (2004) proposed a two-dimensional (2D) wavelet-FEM. Mitra and Gopalakrishnan (2006a, 2006b, 2006c, 2006d, 2006e) proposed several formulations of the wavelet-based spectral finite element to perform wave characteristics and wave propagation in carbon nanotubes. Jin and Xue (2006) developed the 2D plate element approach without tensor product calculation.

In the aforementioned wavelet-FEM applications, the wavelet formulation depends strongly on the specific boundary conditions and they generally lack the ability to solve

problems involving non-homogeneous boundary conditions. Addressing this shortcoming, Zhou and Zhou (2008) developed a modified wavelet-FEM to solve dynamic, static and buckling problems of square plate without requiring specific boundary conditions. Li and Cao (2011) applied later the 1D Daubechies wavelet-FEM to structural response analysis (Li and Cao, 2011).

The spline wavelet-FEM was first applied to the solution of first-kind integral equations on a bounded interval (Goswami, Chan, Chui, 1995). Compared to the Daubechies wavelet, the spline wavelet involves explicit expressions than can be used for the calculation of derivatives and integrals. Additionally, the method was applied to structural mechanics — the wavelet functions were treated as the element displacement interpolation functions to form different types of elements, such as the beam element, the in-plane element, the tetrahedral solid element, and the hexahedral solid element (Han and Ren, 2006, 2009). Several researchers (Xiang and Chen, 2008; Chen and Xiang, 2010; Zhong and Xiang; 2011) conducted a series of studies of multiscale adaptive wavelet-FEM that were constructed using B-spline wavelets on the interval (BSWI) to solve structural analysis and stability analysis problems in 2D and 3D.

The wavelet-FEM, and mostly its BSWI variant, has also been applied to the solution of multiple engineering problems, such as the identification of a crack in a beam (Xiang and Chen, 2006); the identification a crack in a rotor system (Xiang and Chen, 2007; Dong and Chen *et al.*, 2009); the multi-damage detection in plate structures (Xiang and Chen, 2012); wave propagation analysis (Chen and Yang *et al.*, 2012); the detection of beam

cracks using modal shape (Xiang and Liang, 2012a, 2012b); and the identification of damage locations in structures, based on the operating deflection shape or the curvature mode shape (Xiang and Matsumoto, 2011, 2012, 2013a, 2013b). Curved shell elements were also formulated using BSWI (Yang and Chen, 2012), which can better fit the geometry of a system with complex shape/geometry than flat shell elements. The method was used in free vibration and buckling analysis (Yang and Chen, 2013), and resulted in fast convergence with fewer degrees of freedom.

In general, the spline wavelet-FEM is a useful tool to conduct structural analysis. Several numerical examples showed its advantages over traditional numerical methods in terms of the rate of convergence and the accuracy of the solution, especially when computing generalized stresses.

The main advantage of the wavelet-based numerical methods is that they can directly form the multiscale approximations from the two-scale relation. However, wavelets are usually defined on the whole square integrable L^2 domain, which poses significant difficult in the description of boundary conditions, often leading to instabilities.

To address the traditional difficulty of wavelet bases construction on irregularly spaced meshes, the second-generation wavelets (SGW) were introduced. These are built in three steps (Sweldens and Schroder, 2000): (a) split: divide the original set into an even subset and an odd subset, (b) predict: the odd subset can be predicted from the neighboring even samples, and (c) update: form a coarse approximation to the original signal.

The second-generation wavelet finite element method that was proposed later was based on the Hermite family. Sudarshan and D'Heedene (2003) applied this method to analyze the static and dynamic responses of a Euler beam. He and Chen *et al.* (2007, 2008) designed SGW, performed multiresolution finite element method studies, constructed an associated adaptive algorithm, and produced hierarchical approximation spaces. Wang and Chen (2010) first proposed an adaptive multiwavelet-Hierarchical method to solve field problems. Wang and Chen also developed an adaptive inverse iteration algorithm to solve structural eigenvalue problems (Wang and Chen, 2011). Quraishi and Sandeep (2011) applied the SGW-FEM to solve elliptic PDEs on 2D triangulations. Wang and Chen, (2012) introduced a SGW variant based on a lifting scheme and derived the related formulation of the SGW-finite element equations based on the equivalent-filter concept. This method eliminated most restrictions and deficiencies of traditional wavelets, and provided significant flexibility in the solution of engineering problems.

1.2.3 Wavelet-Boundary Element Method

The boundary element method (BEM) reduces the dimensionality of the problems for which it is used, and is generally more accurate than the weighted residual method and FEM. However, the BEM formulation matrices are fully populated and are thus more difficult to solve. This means that the computational time and storage will grow with the square of the domain size. In an effort to create sparse (instead of the fully-populated) boundary element matrices, Spasojevic and Schneider (1997) used the orthogonal Haar wavelet, which resulted in sparse matrices in the solution of the Laplace equation in 2D electrostatic problems.

Koro and Abe (2001a, 2001b) used the non-orthogonal spline wavelet and the orthogonal Haar wavelet to build h-hierarchical BEM for the solution of 2D Laplace problems. Harbrecht and Paiva (2002) developed a multiscale bi-orthogonal wavelet method by coupling FEM and BEW, and applied it to the solution of the 2D Poisson equation. To further reduce the computational load, fast wavelet transforms using parallel iterative methods were introduced to the solution of BEM systems (Gonzalez and Cabaleiro, 2002). Tausch (2003) solved problems of potential theory and Stokes flow problems using a variable order wavelet-BEM. Koro and Abe (2003) proposed a strategy based on wavelet-BEM to determine optimal threshold parameters. Bucher *et al.* (2003) proposed a fast method using assembled BEM matrices and fast wavelet transforms to rapidly solve problems involving multiple load cases. Further developing this scheme, Bucher *et al.* (2004) introduced a computational procedure based on block wavelet transforms.

Eppler and Harbrecht (2003) solved some elliptic shape optimization problems using a wavelet-BEM. The method was further applied to fluid dynamics (Ravnik *et al.*, 2004) using Haar wavelet matrix compression. Ravnik *et al.* (2006, 2008) extended the original method and introduced a hybrid FEM-BEM approach to solve the Navier-Stokes equations and to simulate dilute particle-laden flow. Xiao *et al.* (2007) solved 2Dl potential problems using Daubechies wavelets with coefficient matrices calculated by fast Fourier transforms (FFT). Barmada (2007) applied this method to diffusion problems with time-dependent fundamental solutions. Eppler and Harbrecht (2008) applied a spline wavelet-BEM to the solution of electromagnetic shaping problems in both 2D and 3D.

Xiao and Tausch (2009a, 2009b, 2009c, 2010) conducted a series of studies on wavelet-BEM that: summarized different compression method; introduced a-posteriori compression strategy; simplified the implementation of wavelet-BEM; linked the wavelet-BEM and the low-rank approximation method; developed a fast wavelet-multipole method; was extended to 3D electrostatic analysis; and solved large-scale Stokes flow problems (Xiao and Ye, 2011).

Wavelets with short compact support and a high order of vanishing moments are useful tools to obtain a high matrix compression rate. Thus, selecting or constructing suitable wavelet bases to meet special engineering needs when using the wavelet-BEM is of great significance.

Thus, the main purpose of this chapter is to offer a complete (to the extent possible) discussion on the subject of wavelet applications in the solution of PDEs -- including their advantages, drawbacks, and future potential development of each wavelet-based numerical method -- and to provide some guidance for my future research path.

1.3 The general PDE for flow through porous media

The single-phase fluid flow through anisotropic and heterogeneous porous media can be described by the following general equation:

$$\nabla \cdot \left[\overrightarrow{k_f} \frac{\rho}{\mu} \left(\nabla p - \rho g \nabla z_g \right) \right] + m = \frac{\partial}{\partial t} \left(\rho \phi \right) \quad \text{..... (1.3.1)}$$

where:

$\overrightarrow{k_f}$ = permeability tensor, m^2

μ = fluid viscosity, Pa-s

g = gravitational acceleration, (=9.806) m/s^2

p = reservoir pressure, Pa

ϕ = porosity, fraction

ρ = fluid density, kg/m^3

t = time, sec

z_g = elevation, m

m = mass entering (leaving) a control volume from a sink (source), $kg/m^3/s$

Here, the permeability tensor usually defined as

$$\overrightarrow{k_f} = \begin{bmatrix} k_{xx} & k_{xy} & k_{xz} \\ k_{yx} & k_{yy} & k_{yz} \\ k_{zx} & k_{zy} & k_{zz} \end{bmatrix} \approx \begin{bmatrix} k_{xx} & 0 & 0 \\ 0 & k_{yy} & 0 \\ 0 & 0 & k_{zz} \end{bmatrix} \quad \text{..... (1.3.2)}$$

The off-diagonal permeability terms can be assumed to be zero only if the coordinate system coincides with the principal directions of the permeability tensor.

Eq. (3.1) applies to all fluids and to all conditions under which Darcy's law is valid. Assuming that the porous media is isotropic and that the fluid is slightly compressible (which means that the liquid compressibility is small and both it and the fluid density remain constant within the pressure range of interest), Eq. (3.1) can be simplified as

$$\nabla \cdot \left[\left(\nabla p - \rho g \nabla z \right) \right] + \frac{\mu}{k_f \rho} m = \frac{\mu}{k_f} \phi c_t \frac{\partial p}{\partial t} \quad \text{..... (1.3.3)}$$

where $c_t = c_{f+} c_r$.

c_t = total compressibility, Pa^{-1}

c_f = fluid compressibility, Pa^{-1}

c_r = rock compressibility, Pa^{-1}

Implicit in Eq. (1.3.3) is the assumption that viscosity is constant, which is a valid approximation for isothermal flows and small pressure changes. Next, assuming that gravity plays a minor role (a valid approximation in highly pressurized, relatively thin formations), Eq. (1.3.3) can be further simplified, yielding the following PDE in the 3D cartesian coordinate space:

$$\frac{\partial^2 p}{\partial x^2} + \frac{\partial^2 p}{\partial y^2} + \frac{\partial^2 p}{\partial z^2} + \frac{m\mu}{k_f \rho} = \frac{\mu \phi c_t}{k_f} \frac{\partial p}{\partial t} \quad \text{..... (1.3.4)}$$

Eq. (1.3.4) is known as the diffusivity equation of a single-phase, slightly compressible fluid in a homogenous and isotropic porous medium. Then, the 1D linear flow linear diffusivity equation without an explicit source or sink term is expressed as

$$\frac{\partial^2 p}{\partial x^2} = \frac{\mu \phi c_t}{k_f} \frac{\partial p}{\partial t} \quad \text{..... (1.3.5)}$$

The dimensionless form of linear flow is derived based on a treatment of the inner boundary (*i.e.*, at the source or sink) that accounts for the fixed constant rate, yielding:

$$\frac{\partial^2 p_D}{\partial x_D^2} = \frac{\partial p_D}{\partial t_D}, \quad (1.3.6)$$

in which the dimensionless variables are defined as

$$p_D = \frac{k_f A}{qB\mu x_e}\left(p_i - p\right),\ t_D = \frac{k_f}{\phi\mu c_t x_e^2}t,\ x_D = \frac{x}{x_e} \quad (1.3.7)$$

where x_e is the total length of x domain, A is the cross-Chapter area, B is the formation volume factor, and q is the constant injection or production rate at the inner boundary.

1.4 Objectives

The main objective of this work is to use wavelet-based (*WB*) *numerical methods to solve problems of fluid flow in homogeneous and heterogeneous porous and fractured media, with particular focus on ultra-low permeability* (ULP) systems such as shale oil and gas reservoirs. The effort aims to use the WB simulation approach to analyse the flow and pressure behavior to the external stimuli of fluid injection and/or withdrawal, and intends to include the following activities:

- To extend the wavelet-Galerkin method (WGM) and wavelet-collocation method (WCM) proposed by Moridis *et al.* (1996) to the solution of two-phase flow problems.
- To derive a general approach involving the use of different appropriate wavelet bases and the application of their multi-resolution property to solve problems of single- and multi-phase flow through multidimensional porous media domains.

- To develop a compact MATLAB program implementing the WB solutions.
- To compare the results obtained from the various WB numerical methods using different wavelet bases.
- To validate the WB solutions against analytical solutions and the predictions of a numerical reservoir simulator.

CHAPTER II

WAVELET TRANSFORMS AND THEIR APPLICATION TO THE SOLUTION OF THE PDE OF FLOW

2.1 General wavelet concepts and approach

2.1.1 Wavelet Function and Scaling Function

In the terminology used in this study, $\psi(x)$ is referred to as a *mother wavelet* or *basic wavelet*. The integral of wavelet function $\psi(x)$ is zero in the interval of $(-\infty,+\infty)$, *i.e.*,

$$\int_{-\infty}^{+\infty}\psi(x)\,dx=0 \quad \text{.....(2.1.1)}$$

Traditionally, wavelets are generated by a scaling factor and a translation factor as follows:

$$\psi_{j,k}=2^{j/2}\psi\left(2^{j}x-k\right)\quad j,k\in\mathbb{Z}, \quad \text{.....(2.1.2)}$$

where $\mathbb{Z}$ is the set of all integers, x is the independent variable of the wavelet, j is the scaling factor, and k is the translation or shifting factor. Moreover, 2^j is the stretch of the wavelet and the factor $2^{j/2}$ maintains a constant norm independent of the scale j. The equation above has also been named as the "two-dimensional parameterization" (Burrus, 1997) achieved by the wavelet function $\psi(x)$.

Wavelet analysis allows a target function to be represented in terms of different wavelet bases over an interval. Thus, theoretically, any function $f(x)$ can be expressed as:

$$f(x)=\sum_{j,k=-\infty}^{\infty}a_{j,k}\psi_{j,k}(x) \quad \text{.....(2.1.3)}$$

where the terms $a_{j,k}$ are called the *wavelet expansion coefficients* and can be calculated from the relationship

$$a_{j,k} = \left\langle f(x), \psi_{j,k}(x) \right\rangle, \quad \text{(2.1.4)}$$

in which $\left\langle A, B \right\rangle$ denotes the inner product of the quantities A and B to the right and left of the comma, respectively.

Generally, the multiresolution formulation requires two closely related basic functions. In addition to the mother wavelet $\psi(x)$ discussed above, the other basic function is the *scaling function* $\varphi(x)$. A set of scaling functions are defined in terms of integer translations of the basic scaling function as follows:

$$\varphi_k(x) = \varphi(x-k), \ k \in \mathbb{Z}, \ \varphi \in L^2(\mathbb{R}) \quad \text{(2.1.5)}$$

where L^2 denotes the space of all functions $\varphi(x)$ with a well-defined integral of the square of the function. Here, L stands for a Lebesque integral, and $\mathbb{R}$ denotes that the integration of the independent variable x is a number over the whole real line.

The subspace V_0 of $L^2(\mathbb{R})$, can be spanned by the translations of the scaling function as

$$V_0 = \overline{\underset{k}{Span}\left\{\varphi_k(x)\right\}}, \ k \in \mathbb{Z} \quad \text{(2.1.6)}$$

The over-bar in Eq. (2.1.6) denotes closure of the associated space. Eq. (2.1.6) means that, for any $f(x) \in V_0$,

$$f(x) = \sum_k a_k \varphi_k(x) \quad \text{(2.1.7)}$$

where, a_k is the coefficient of each translation of the basic scaling function.

Next, by changing the scale of the scaling function, the size of each subspace can be increased. A family of scaling functions can then be generated from the basic scaling function $\varphi(x)$ by scaling and translation, yielding:

$$\varphi_{j,k}(x) = 2^{j/2}\varphi\left(2^j x - k\right) \quad j,k \in \mathbb{Z} \qquad (2.1.8)$$

The new subspace V_j spanning over *k* is:

$$V_j = \overline{\underset{k}{Span}\left\{\varphi_k\left(2^j x\right)\right\}} = \overline{\underset{k}{Span}\left\{\varphi_{j,k}(x)\right\}},\ k \in \mathbb{Z} \qquad (2.1.9)$$

The term $\left\{\varphi_{j,k}(x)\right\}_{k\in\mathbb{Z}}$ forms a Riesz basis of V_j. For any $f(x) \in V_j$:

$$f(x) = \sum_k a_k \varphi\left(2^j x + k\right) \qquad (2.1.10)$$

For $j > 0$, the size of the span will be larger than the span in Eq. (2.1.6) because $\varphi_{j,k}(x)$ is narrower than $\varphi_k(x)$ in Eq. (2.1.6). The new span in Eq. (2.1.10) can represent the finer details of a function. On the contrary, for $j < 0$, the spanned subpace is smaller than the span in Eq. (2.1.6) because $\varphi_{j,k}(x)$ is wider than $\varphi_k(x)$ in Eq. (2.1.6), which represents only coarse information on a function.

2.1.2 Multiresolution Analysis

The multiresolution property of wavelets is an important property that can be exploited for the multilevel approximation of problems of flow and geomechanics routinely

encountered in petroleum engineering. A multiresolution analysis is composed of a nest of closed subspaces $\left(V_j\right)_{j\in\mathbb{Z}} \in L^2\left(\mathbb{R}\right)$ such that:

(i) $V_j \subset V_{j+1}$

(ii) $f\left(x\right)\in V_j \Leftrightarrow f\left(2x\right)\in V_{j+1},\ j\in\mathbb{Z}$

(iii) $f\left(x\right)\in V_j \Leftrightarrow f\left(x-2^{-j}\right)\in V_j,\ j\in\mathbb{Z}$

(iv) $\underset{j\in\mathbb{Z}}{\cup} V_j$ is dense in $L^2\left(\mathbb{R}\right)$, and $\underset{j\in\mathbb{Z}}{\cap} V_j = \left\{0\right\}$

(v) There is a function $\varphi\in V_0$, such that $\left\{\varphi\left(x-k\right)\right\}_{k\in\mathbb{Z}}$ forms a Riesz basis of V_0

The first property (i) is simply called the nested property, which indicates that the space that contains the high-resolution functions will also contain those of a lower resolution. The second property (ii) is called self-similarity in scale *j*, which ensures that the elements in space V_j are simply scaled versions of the elements in the next finer space V_j. Similarly, the third property (iii) describes self-similarity in the independent variable *x*. Each subspace V_j is invariant under translations or shifts of 2^{-j}.

The fourth property (iv) is named completeness and demands that the union of the nested subspaces fill the whole space; in other words, to be dense in $L^2(\mathbb{R})$. Additionally, the intersection of those subspaces only contains the zero element, *i.e.*, they do not include redundant information.

The fifth property (v) is named regularity and requires that the subspace V_0 be generated as the linear span of the integer shifts *k* of a finite number of the basic scaling function

$\varphi(x)$. It also imposes certain conditions, *i.e.*, there exist constants c $(0 < c \le C < +\infty)$ such that:

$$c\left(\sum_{k\in\mathbb{Z}}|a_k|^2\right) \le \left\|\sum_{k\in\mathbb{Z}} a_k\varphi(x-k)\right\|_2^2 \le C\left(\sum_{k\in\mathbb{Z}}|a_k|^2\right) \quad \text{..... (2.1.11)}$$

for all sequences of a_k in the space l^2.

Therefore, the scaling function $\varphi(x)$ generates a multiresolution analysis (MRA) with the properties discussed above.

2.2 The Haar wavelets

Mathematically, Haar wavelets are a sequence of rescaled "square-shaped" functions that were proposed by Haar (1910). The "mother" wavelet function and the associated scaling function of the Haar wavelet are defined as follows:

$$\psi(x) = \begin{cases} 1 & 0 \le x < \frac{1}{2} \\ -1 & \frac{1}{2} \le x < 1 \\ 0 & \text{otherwise} \end{cases} \quad \text{..... (2.2.1)}$$

$$\varphi(x) = \begin{cases} 1 & 0 \le x < 1 \\ 0 & \text{otherwise} \end{cases} \quad \text{..... (2.2.2)}$$

Graphs of these functions are shown in **Fig. 2.1.**

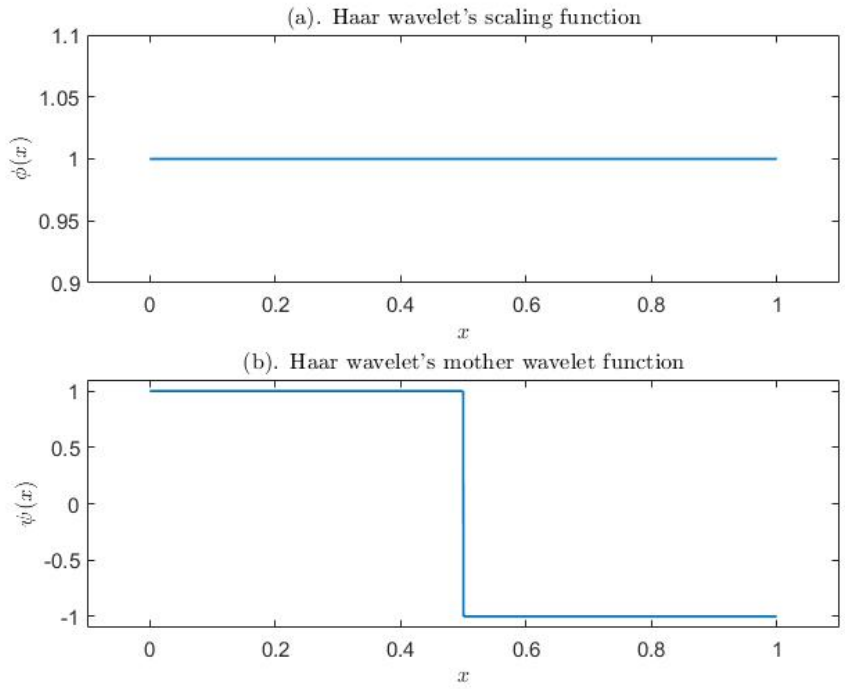

Figure 2.1 – (a) Haar wavelet's scaling function φ(x), and (b) Haar wavelet's mother wavelet function ψ(x).

The Haar wavelet family on an interval $x \in \left[\zeta_1, \zeta_2\right]$ is described by

$$h_i\left(x\right) = \begin{cases} 1 & \xi_1 \le x < \xi_2 \\ -1 & \xi_2 \le x < \xi_3 \\ 0 & \text{otherwise} \end{cases} \quad \text{..... (2.2.3)}$$

where *h* denotes the Haar wavelet family, and the subscript *i* indicates the i-th Haar wavelet.

The subdomain parameters ξ are defined as:

$$\xi_1 = \zeta_1 + \frac{(\zeta_2 - \zeta_1)}{2m}(2k)$$
$$\xi_2 = \zeta_1 + \frac{(\zeta_2 - \zeta_1)}{2m}(2k+1) \quad \text{..... (2.2.4)}$$
$$\xi_3 = \zeta_1 + \frac{(\zeta_2 - \zeta_1)}{2m}(2k+2)$$

where

$$m = 2^j$$
$$j = 0,\ 1,\ ...,\ J \quad \text{..... (2.2.5)}$$
$$k = 0,\ 1,\ ...,\ m-1$$

and J is defined as the maximum level of resolution:

The scaling parameter j and the shift parameter k were discussed in **Section 2.1.1**.

Given Eq. (2.2.5), the number of wavelets i can be obtained as $i = m + k + 1$. Note that j is also named the *level of resolution*: as j increases to a maximum level of resolution J, the wavelet becomes narrower. The translation factor k localizes the position of the wavelet on the x-axis. When k increases from 0 to $m-1$ on the x-axis, the initial point ξ_i of the i-th Haar wavelet $h_i(x)$ changes from ζ_1 to $\frac{\zeta_1 + (m-1)\zeta_2}{m}$.

Eq. (2.2.3) is valid only if $i > 2$. The case for $i = 1$ corresponds to the scaling function of the Haar wavelet that was introduced by Eq. (2.2.2) and **Fig. 2.1**(**b**). **Fig. 2.2** presents four examples of the Haar wavelet family, that is from $h_1(x)$ to $h_4(x)$ on the domain $x \in [0,1]$ (*i.e.*, with i varying from 1 to 4) and for various values of j and k.

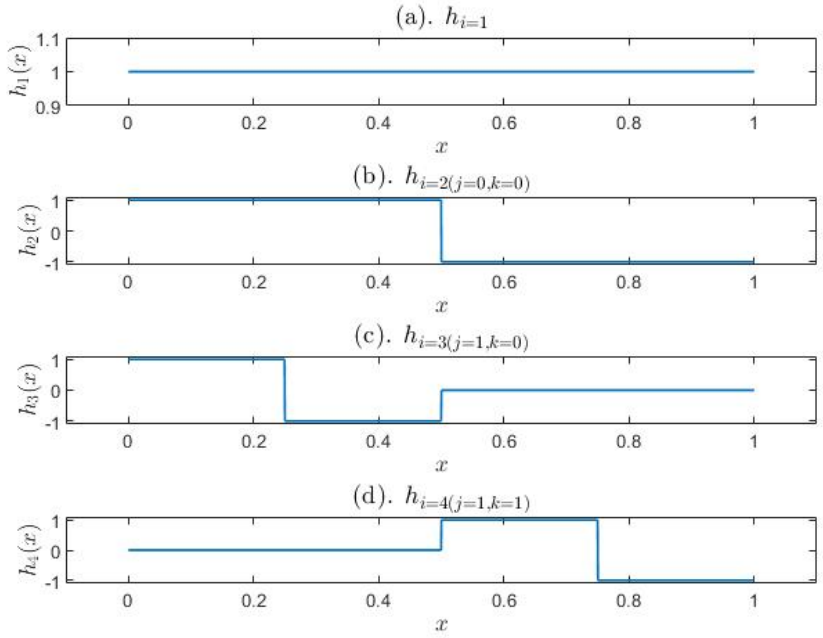

Figure 2.2 – Haar wavelet for (a) i = 1; (b) i = 2, j = 0, k = 0; (c) i =3, j = 1, k = 0; (d) i = 4, j = 1, k = 1

Select integrals of the Haar wavelets are as follows:

$$I_{i,1} = \int_0^x h_i(x)\,dx$$
$$I_{i,2} = \int_0^x I_{i,1}(x)\,dx \quad \text{..... (2.2.6)}$$

in which I denotes an integral of a Haar wavelet, the first subscript i indicates the integral of the i-th Haar wavelet family, and the second subscript denotes the number of times of integration. Those formulas hold true for any $i > 1$.

Based on Eq. (2.2.3), it is easy to obtain the following explicit expressions for those integrals on $x \in [\zeta_1, \zeta_2]$:

$$I_{i,1}(x)=\begin{cases}0 & \zeta_1 \le x < \xi_1 \\ x-\xi_1 & \xi_1 \le x < \xi_2 \\ \xi_3 - x & \xi_2 \le x < \xi_3 \\ 0 & \xi_3 \le x < \zeta_2 \end{cases} \quad \text{..... (2.2.7)}$$

$$I_{i,2}(x)=\begin{cases}0 & \zeta_1 \le x < \xi_1 \\ \dfrac{(x-\xi_1)^2}{2} & \xi_1 \le x < \xi_2 \\ \dfrac{(x-\xi_1)^2-2(x-\xi_2)^2}{2} & \xi_2 \le x < \xi_3 \\ \dfrac{(x-\xi_1)^2-2(x-\xi_2)^2+(x-\xi_3)^2}{2} & \xi_3 \le x < \zeta_2 \end{cases} \quad \text{..... (2.2.8)}$$

The integrals $I_{i,1}(x)$ and $I_{i,2}(x)$ corresponding to the wavelets h_1 to h_4 (shown in **Fig. 2.2**) are presented in **Figs. 2.3** and **2.4**, respectively.

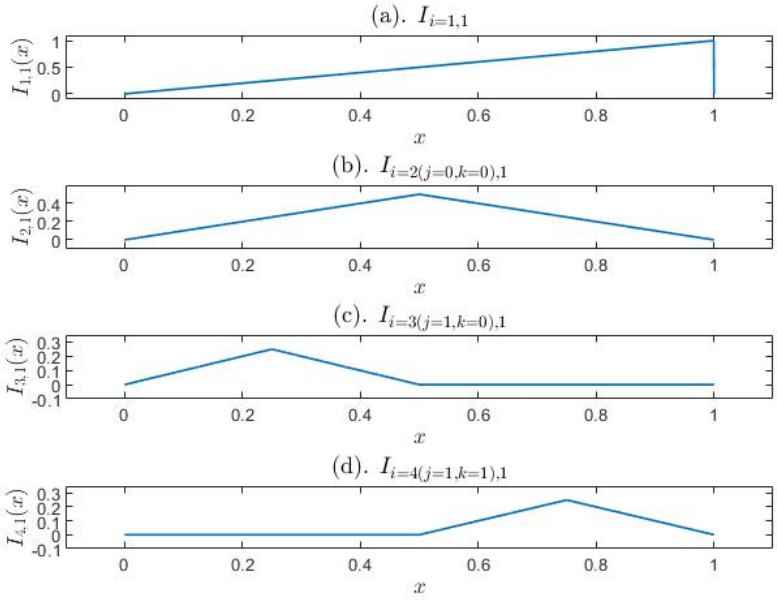

Figure 2.3 – Integrals Ii,1(i = 1, … ,4) of the Haar wavelets shown in Fig. 2.2.

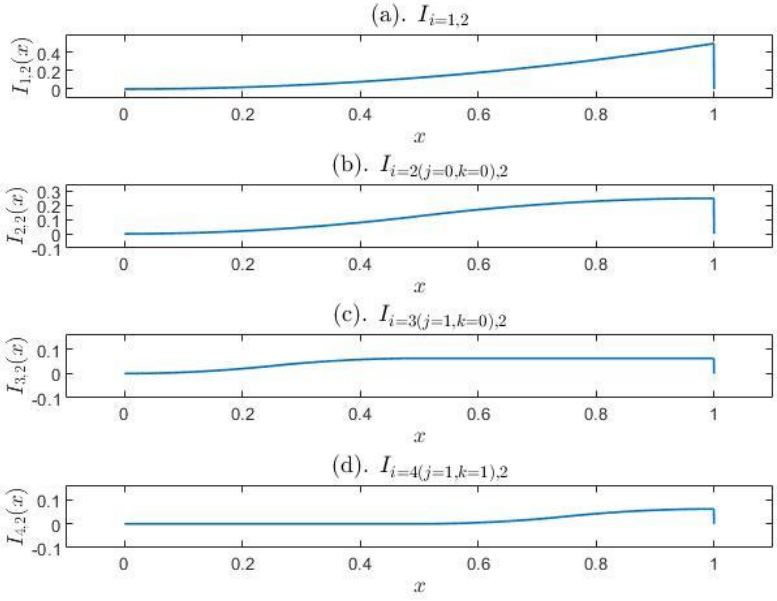

Figure 2.4 – Integrals $I_{i,2}$ (i = 1, … ,4) of the Haar wavelets shown in Fig. 2.2.

2.3 The B-spline wavelets

B-splines are a special type of cardinal splines. They are defined by the following recursive formula:

$$N_m(x) = \int_{-\infty}^{\infty} N_{m-1}(x-t)\, N_1(x)\, dt \quad \text{..... (2.3.1)}$$

$$N_1(x) = \begin{cases} 1 & 0 \le x < 1 \\ 0 & o.w. \end{cases} \quad \text{..... (2.3.2)}$$

where $N_m(x)$ is the B-spline of order *m*, with *m* being any positive integer.

The cardinal B-splines start from the B-spline of order $m = 1$, which is the constant B-spline that takes the value 1 in the interval [0,1] and 0 elsewhere. This is the reason why the linear spline (usually associated with the exponent 1) corresponds to $m = 2$, and the cubic spline (usually associated with the exponent 3) corresponds to $m = 4$.

Chui and Wang (1991, 1992a, 1992b, 1993) developed B-spline wavelets bases using B-spline functions. B-spline wavelet applications often involve splines with an even order *m*. At this point, we present information describing the difference in behavior between linear ($m = 2$) and cubic B-spline wavelets ($m = 4$).

The linear B-spline function $N_2(x)$ is given by:

$$N_2(x) = \begin{cases} x & 0 \le x < 1 \\ -x+2 & 1 \le x < 2 \\ 0 & o.w. \end{cases} \quad \text{..... (2.3.4)}$$

In the ensuing discussion, the resolution level *j* and the dilation parameter *k* are as they have been earlier defined in Chapters **2.1** and **2.2.** For B-spline wavelets, the range of *k* is

in the domain $\left[1-m, 2^n-1\right]$. Using the *j* and *k* values in the four examples of **Fig. 2.2**, the corresponding linear B-spline wavelets family N_2 in the domain $x \in [-1, 2]$ is shown in **Fig. 2.5**. Note that, when $j = 0$ in **Fig. 2.5(a)**, *i.e.*, when resolution level is zero, the resulting plot describes the linear B-spline scaling function itself; when the resolution level $j = 1$, the wavelet is narrower by a factor of 2 and is shifted from $k = -1$ to $k = 1$ – see **Figs. 2.5(b)** to **Fig. 2.5(d)**.

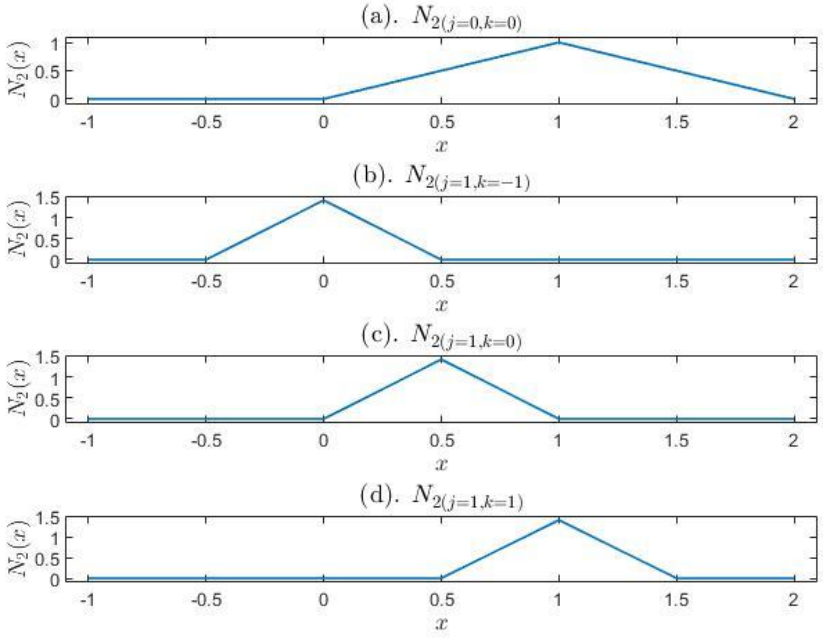

Figure 2.5 – Linear B-spline wavelet for (a) $j = 0$, $k = 0$; (b) $j = 1$, $k = -1$; (c) $j = 1$, $k = 0$ (d) $j = 1$, $k = 1$

Here, $N_2(x)$ is in essence the scaling function $\varphi(x)$ of the linear spline wavelets. Recalling Eq. (2.1.8) that defined a family of scaling functions, the scaling function of the linear B-spline wavelet family in the example of **Fig. 2.5** is described as:

$$\varphi(x) = N_m(x) = \sum_{k=0}^{m} 2^{-m+1} \binom{m}{k} \varphi(2x-k) \quad \text{..... (2.3.5)}$$

and the wavelet basis $\psi(x)$ is given by

$$\psi(x) = 2^{-m+1} \sum_{k=0}^{2m-2} (-1)^k N_{2m}(k+1) N_{2m}^{(m)}(2x-k) \quad \text{..... (2.3.6)}$$

where, $N_{2m}^{(m)}(2x-k) = \sum_{k=0}^{m} (-1)^k \binom{m}{k} \phi(x-k)$.

Because of the superior accuracy and flexibility that makes cubic spline wavelets convenient to use, these are used as the basis in the WB solution for the PDEs of interest in petroleum engineering. Also, Haar wavelets are included for the purposes of completeness and comparison of performance.

The scaling function of the cubic spline wavelet function is defined as follows:

$$N_4(x) = \begin{cases} \frac{1}{6}x^3, & 0 \le x_j < 1 \\ -\frac{1}{2}x^3 + 2x^2 - 2x + \frac{2}{3}, & 1 \le x_j < 2 \\ \frac{1}{2}x^3 - 4x^2 + 10x - \frac{22}{3}, & 2 \le x_j < 3 \\ -\frac{1}{6}x^3 + 2x^2 - 8x + \frac{32}{3}, & 3 \le x_j < 4 \\ 0, & \text{otherwise} \end{cases} \quad \text{..... (2.3.7)}$$

Fig. 2.6 presents six examples of the cubic B-spline wavelet family (m = 4) for various j and k values. For zero-level resolution (j = 0) in **Fig. 2.6**(**a**), N_4 is in essence the cubic B-

spline function, namely the scaling function that generates MRA; for j = 1, the wavelet is narrower for a factor of 2 and is shifted from k = -3 to k = 1.

The interpolation wavelets that generate B-spline wavelets are not compactly supported. Compactly supported B-spline wavelets were developed by Chui and Wang (1991, 1992a, 1992b, 1993). The Chui-Wang wavelets, denoted as $\psi_{j,k}(x)$, have the following properties:

(i) These are smooth in $\mathbb{C}^k$

(ii) These are semi-orthogonal: $<\psi_{jk},\ \psi_{j'k'}>=0,\ \ j \neq j'\ \ j, j', k, k' \in \mathbb{Z}$

(iii) $\psi_{j,k}(x)$ is symmetric for an even spline order *m*, and anti-symmetric for an odd spline order *m*

(iv) The support of $\psi_{j,k}(x)$ is in the closed interval $\left[2^{-j}k,\ 2^{-j}\left(k+2m-1\right)\right]$

One major advantage of B-spline wavelets is that explicit expressions exist for the scaling function, the wavelet function and their dual functions. A disadvantage is that the dual wavelet function and scaling function are not compactly supported.

2.4 WB Solution of the 1D Equation of Flow

2.4.1 Haar WB Solution

Recalling Eq. (2.1.7), any square integrable function $f(x)$ in the interval [0,1] can be expressed as:

$$f(x)=\sum_{i=1}^{\infty} a_i h_i(x) \quad \text{.....} \quad (2.4.1)$$

where the coefficients $a_i = 2^j \int_0^1 f(x) h_i(x) dx$, and $h_i(x)$ is the i-th Haar wavelet.

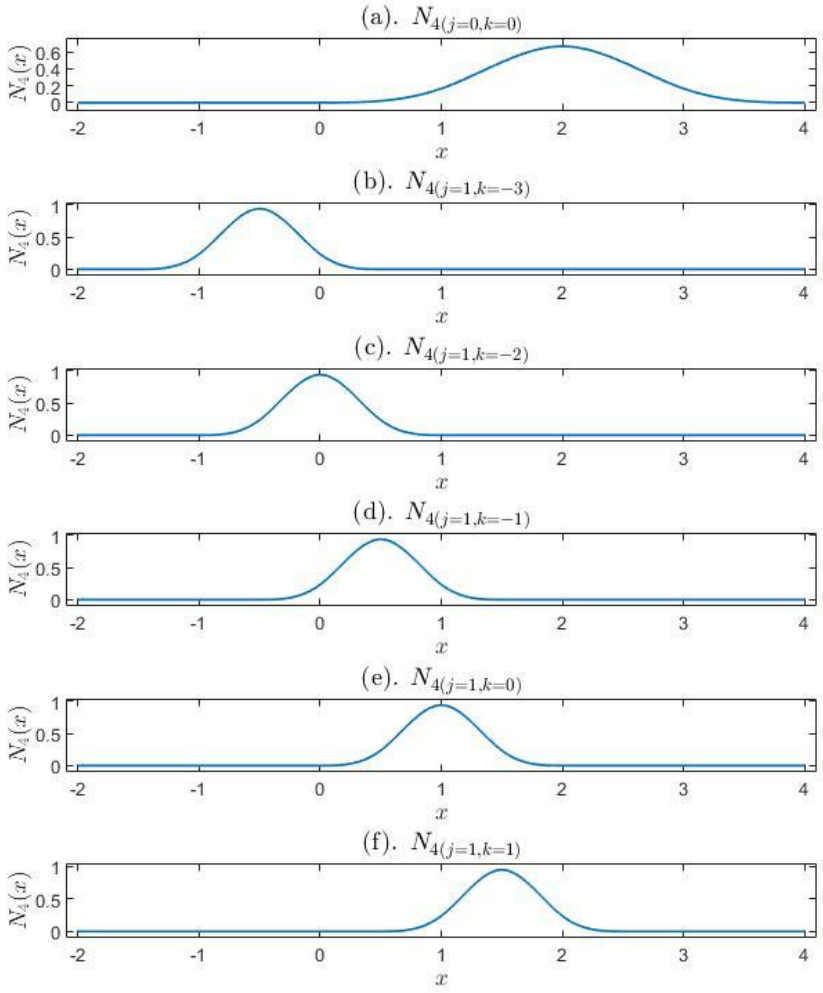

Figure 2.6 – Cubic B-spline wavelet for (a) *j* = 0, *k* = 0; (b) *j* = 1, *k* = -3; (c) *j* = 1, *k* = -2 (d) *j* = 1, *k* = -1; (e) *j* = 1, *k* = 0; (f) *j* = 1, *k* = 1

Assuming that the function $f(x)$ can be approximated as piecewise-constant in each sub-interval, the infinite number of terms is drastically reduced to a limited number of finite terms. Therefore,

$$f(x) = \sum_{i=1}^{2M} a_i h_i(x) = a_{2M}^T h_{2M}(x) \quad \text{..... (2.4.2)}$$

where, $M = 2^J$, J is the maximum resolution level defined earlier in Eq. (2.2.5), T denotes the transpose of the associated vector, and the coefficients and Haar wavelet family are column vectors expressed as follows:

$$\begin{aligned} a_{2M}^T &= [a_1,\ a_2,\ ...,\ a_{2M}] \\ h_{2M}(x) &= [h_1(x),\ h_2(x),\ ...,\ h_{2M}(x)]^T \end{aligned} \quad \text{..... (2.4.3)}$$

The 1D flow in the x-direction of a nearly incompressible fluid through a homogeneous porous medium is described by the following diffusivity partial differential equation (PDE):

$$\frac{\partial^2 p}{\partial x^2} = \frac{\mu \phi c_t}{k_f} \frac{\partial p}{\partial t} + \frac{\tilde{q}_{sc}}{\lambda} \quad \text{..... (2.4.4)}$$

$\tilde{q}_{sc} = \dfrac{\tilde{m}}{\rho_{sc}}$ is the strength of the source or sink

λ = $k/(\mu B)$ is the mobility.

$\tilde{q}_{sc}$ = permeability tensor, s^{-1}

ρ_{sc} = fluid density at standard condition, kg/m^3

λ = mobility, $m^2/Pa/s$

B = formation volume factor, res vol/std vol

From Eq. (1.3.6) in **Section 1.3**, the dimensionless form of the PDE in Eq. (1.6) is:

$$\frac{\partial^2 p_D}{\partial x_D^2} = \frac{\partial p_D}{\partial t_D}$$

with the initial condition of $p_D(x_D, t_D = 0) = 0$ and boundary conditions that are described as follows:

$$\frac{\partial p_D}{\partial x_D}(x_D = 0, t_D) = -1 \quad \text{..... (2.4.5)}$$

$$p_D(x = 1, t_D) = 0 \quad \text{..... (2.4.6)}$$

where Eq. (2.4.5) describes a constant production rate at the inner boundary (*i.e.*, the well), and Eq. (2.4.6) describes a no-flow outer boundary of the domain.

The dimensionless variables p_D, x_D and t_D are defined in Eq. (1.3.7).

The spatial and temporal discretization of the diffusivity equation in Eq. (1.3.6) is now discussed. For $x_D \in [0,1]$, the grids are defined by: $x_D^l = \frac{l - 0.5}{2M}$, $l = 1, 2, ..., 2M$, in which the subscript *D* denotes a dimensionless variable, and the superscript *l* denotes the level of discretization (refinement) of each one of the *2M* grids. For $t_D \in [t_{st}, t_{end}]$, time is divided into N_t segments of equal length $\Delta t = \frac{t_{end} - t_{st}}{N_t}$, where t_{st} denotes the starting point in time (usually t_{st} = 0) and t_{end} denotes the ending time. The timesteps define the series of discretized times $t_D^s = (s-1)\Delta t$, $s = 1, 2, ..., N_t$, where Δt denotes the increment/ timestep (into which time is subdivided), and *s* is the timestep number in the sequence.

To solve the 1D fluid flow through porous media problem, the time-dependent right-hand side (RHS) of Eq. (1.3.6) is discretized using a standard backward Finite-Difference (FD) scheme, which yields:

$$\frac{\partial^2 p_D}{\partial x_D^2}\left(x_D, t_D^{s+1}\right) = \frac{p_D\left(x_D, t_D^{s+1}\right) - p_D\left(x_D, t_D^{s}\right)}{\Delta t} \quad \text{..... (2.4.7)}$$

Following the approach of Lepik (2005, 2007), at each time subinterval $t_D \in \left[t_D^s, t_D^{s+1}\right]$, the left-hand side (LHS) of Eq. (1.3.6) $\frac{\partial^2 p_D}{\partial x_D^2}\left(x_D, t_D^{s+1}\right)$ is approximated by a series of Haar wavelets using Eq. (2.4.2), resulting in:

$$\frac{\partial^2 p_D}{\partial x_D^2}\left(x_D, t_D^{s+1}\right) = \sum_{i=1}^{2M} a_i h_i\left(x_D\right) \quad \text{..... (2.4.8)}$$

Integrating Eq. (2.4.8) with respect to x_D from 0 to x_D yields:

$$\frac{\partial p_D}{\partial x_D}\left(x_D, t_D^{s+1}\right) = \frac{\partial p_D}{\partial x_D}\left(0, t_D^{s+1}\right) + \sum_{i=1}^{2M} a_i I_{i,1}\left(x_D\right) \quad \text{..... (2.4.9)}$$

where the $\frac{\partial p_D}{\partial x_D}\left(0, t_D^{s+1}\right)$ term is known because of the given inner boundary condition.

Next, integration of Eq. (2.4.9) from 0 to x_D results in:

$$p_D\left(x_D, t_D^{s+1}\right) = p_D\left(0, t_D^{s+1}\right) + \left(x_D - 0\right) \cdot \frac{\partial p_D}{\partial x_D}\left(0, t_D^{s+1}\right) + \sum_{i=1}^{2M} a_i I_{i,2}\left(x_D\right) \quad \text{..... (2.4.10)}$$

To find the unknown $p_D\left(0,t_D^{s+1}\right)$, $x_D=1$ is substituted into Eq. (2.4.10) to obtain:

$$p_D\left(1,t_D^{s+1}\right)=p_D\left(0,t_D^{s+1}\right)+(1-0)\cdot\frac{\partial p_D}{\partial x_D}\left(0,t_D^{s+1}\right)+\sum_{i=1}^{2M}a_iI_{i,2}(1) \quad \text{..... (2.4.11)}$$

Substitution of the inner boundary conditions in Eqs. (2.2.5) and (2.2.6) into Eq. (2.4.11), provides the unknown $p_D\left(0,t_D^{s+1}\right)$ as:

$$p_D\left(0,t_D^{s+1}\right)=1-\sum_{i=1}^{2M}a_iI_{i,2}(1) \quad \text{..... (2.4.12)}$$

Substitution of Eq. (2.4.12) and the inner boundary condition given by Eqs. (2.2.5) and (2.2.6) into Eq. (2.4.10) provides the general wavelet-based expression for pressure at time t_D^{s+1} as:

$$p_D\left(x_D,t_D^{s+1}\right)=(1-x_D)+\left(\sum_{i=1}^{2M}a_iI_{i,2}(x_D)-\sum_{i=1}^{2M}a_iI_{i,2}(1)\right) \quad \text{..... (2.4.13)}$$

Next, inserting Eqs. (2.4.8) and (2.4.13) into Eq. (2.4.7) and rearranging terms leads to the following equation:

$$\sum_{i=1}^{2M}a_i\left[h_i(x_D)\cdot\Delta t-I_{i,2}(x_D)+I_{i,2}(1)\right]=(1-x_D)-p_D\left(x_D,t_D^s\right) \quad \text{..... (2.4.14)}$$

When $s=0$, $t_D^s=t_{st}=0$, $p_D\left(x_D,t_D^s\right)$ is given by the initial condition $p_D\left(x_D,t_D=0\right)=0$ and the boundary grid points are constrained by the known boundary conditions. Then the coefficients a_i of Eq. (2.4.14) can be successively calculated, with the estimation process starting with the known initial condition.

2.4.2 Cubic B-spline WB Solution

The $p_D(x_D,t_D)$ in the 1D dimensionless form of the diffusivity Eq. (1.3.6) that describes flow through a homogeneous porous media, as well as in the corresponding initial and boundary conditions described by Eqs. (2.2.5) and (2.2.6), is approximated by a finite series of cubic B-spline scaling functions $\varphi_{j,k}(x_D)$ as:

$$p_D(x_D,t_D)=\sum_k a_{j,k}(t_D)\varphi_{j,k}(x_D) \quad \text{..... (2.4.15)}$$

where, $a_{j,k}(t_D)$ are the coefficients of each of the cubic B-spline scaling functions. The resolution level *j* and *k* are as previously defined.

Because the cubic B-spline scaling functions and their first and second derivatives have explicit expressions, the second derivative of the dimensionless pressure function with respect to x-axis can be easily expressed as follows:

$$\frac{\partial^2 p_D}{\partial x_D^2}(x_D,t_D)=\sum_k a_{j,k}(t_D)\frac{d^2\varphi_{j,k}}{dx_D^2}(x_D) \quad \text{..... (2.4.16)}$$

Similarly, for $x_D \in [0,1]$, the interval Δx between two consecutive points on the x-axis is defined as $\Delta x=\frac{1}{N_x}$, where N_x denotes the number of the equally spaced grid points. Each point in the discretized domain is defined as $x_D^l=(l-1)\Delta x,\ l=1,2,...,N_x$, where superscript *l* denotes the number of the discretized interval in the Δx sequence.

The time discretization follows the same approach described in the case of the Haar WB solution of the 1D diffusivity. Thus, the temporal discretization of the RHS of the PDE in Eq. (1.3.6) and substitution of Eqs. (2.4.15) and (2.4.16) therein yields:

$$\sum_k a_{j,k}\left(t_D^{s+1}\right)\frac{d^2\varphi_{j,k}}{dx_D^2}\left(x_D\right)=\frac{\sum_k a_{j,k}\left(t_D^{s+1}\right)\varphi_{j,k}\left(x_D\right)-\sum_k a_{j,k}\left(t_D^{s}\right)\varphi_{j,k}\left(x_D\right)}{\Delta t} \quad \text{..... (2.4.17)}$$

Rearrangement of Eq. (2.4.17) results in:

$$\sum_k a_{j,k}\left(t_D^{s+1}\right)\left[\Delta t\cdot\frac{d^2\varphi_{j,k}}{dx_D^2}\left(x_D^l\right)-\varphi_{j,k}\left(x_D^l\right)\right]=\sum_k a_{j,k}\left(t_D^{s}\right)\varphi_{j,k}\left(x_D^l\right) \quad \text{..... (2.4.18)}$$

Because of the known initial and boundary conditions of Eq. (2.4.15), the RHS of Eq. (2.4.18) is known. This allows the determination of the coefficients $a_{j,k}\left(t_D^{s+1}\right)$ for each time t_D^{s+1} of the sequence of timesteps into which the time dimension is discretized.

2.5 WB Solution of the 2D Equation of Flow

Multidimensional wavelet bases can be constructed from one-dimensional wavelet bases or scaling functions by means of a tensor product (Mallat, 1989). In this case, the scaling functions for the 2D case are:

$$\Phi_{j,k_1,k_2}(x,y)=\varphi\otimes\varphi(x,y)=\varphi_{j,k_1}(x)\varphi_{j,k_2}(y) \quad \text{..... (2.3.1)}$$

where k_1 and k_2 are shifting factors of the scaling functions corresponding to the independent variable x and y, respectively. The symbol $\otimes$ denotes a Kronecker product.

Similarly, 2D wavelets are defined by the following three different sets of equations:

$$\Psi^{(1)}_{j,k_1,k_2}(x,y) = \varphi \otimes \psi(x,y) = \phi_{j,k_1}(x)\psi_{j,k_2}(y)$$
$$\Psi^{(2)}_{j,k_1,k_2}(x,y) = \psi \otimes \varphi(x,y) = \psi_{j,k_1}(x)\phi_{j,k_2}(y) \quad \text{..... (2.3.2)}$$
$$\Psi^{(3)}_{j,k_1,k_2}(x,y) = \psi \otimes \psi(x,y) = \psi_{j,k_1}(x)\psi_{j,k_2}(y)$$

The flow of a nearly incompressible fluid through a 2D homogeneous and isotropic porous medium is described by the following diffusivity PDE, already discussed in a more general form in Eq. (1.3.4) of **Section 1.3**:

$$\frac{\partial^2 p}{\partial x^2} + \frac{\partial^2 p}{\partial y^2} = \frac{\mu\phi c_t}{k_f}\frac{\partial p}{\partial t} + \frac{m}{\rho_{sc}\lambda}, \quad x \in [0, x_e], y \in [0, y_e], t \geq 0 \quad \text{..... (2.3.3)}$$

The x and y coordinates are normalized first, resulting in the dimensionless coordinates: $x_D = \frac{x}{x_e}, y_D = \frac{y}{y_e}$ and $(x_D, y_D) \in (0,1)\times(0,1)$. Similarly, the initial and boundary conditions are defined in terms of the dimensionless coordinates as:

$$\frac{\partial p}{\partial x_D}(0, y_D, t_D) = g_1(y_D); \quad \frac{\partial p}{\partial x_D}(1, y_D, t_D) = g_2(y_D);$$
$$\frac{\partial p}{\partial y_D}(x_D, 0, t_D) = g_3(x_D); \quad \frac{\partial p}{\partial y_D}(x_D, 1, t_D) = g_4(x_D); \quad \text{..... (2.3.4)}$$
$$p(x_D, y_D, 0) = f(t_D)$$

where $g_i(u)$, i = 1, 2, 3, 4 denotes a Neumann boundary condition function, $f(v)$ denotes an initial condition function, and u and v are the general independent variables of the corresponding functions.

Using cubic B-spline basis, we approximate the pressure term as:

$$p(x_D, y_D, t) \approx \sum_k a_{j,k_1,k_2}(t)\Phi_{j,k_1,k_2}(x_D, y_D) \quad \text{..... (2.3.5)}$$

In a manner entirely analogous to that for the solution of the 1D PDE, for $x_D \in [0,1]$ and $y_D \in [0,1]$, the intervals Δx and Δy between any two successive points on the *x*- and *y*-axes, respectively, are defined as $\Delta x = \frac{1}{N_x}$, $\Delta y = \frac{1}{N_y}$, where N_x and N_y denote the number of subdivisions into which the *x*- and the *y*-axes are discretized. Time is discretized in a manner identical to that in the 1D PDE and will not be further discussed here.

Spatial and temporal discretization of Eq. (2.3.3) and substitution of Eq. (2.3.5) using cubic B-spline wavelets, yields:

$$\begin{aligned}
&\frac{1}{x_e^2}\sum_k a_{j,k_1,k_2}\left(t^{j+1}\right)\frac{\partial^2 \varphi_{j,k_1}}{\partial x_D^2}\left(x_D\right)\varphi_{j,k2}\left(y_D\right) \\
&+\frac{1}{y_e^2}\sum_k a_{j,k_1,k_2}\left(t^{j+1}\right)\varphi_{j,k1}\left(x_D\right)\frac{\partial^2 \varphi_{j,k_2}}{\partial y_D^2}\left(y_D\right) \\
&= \frac{\mu\phi c_t}{\Delta t k_f}\left[\begin{array}{l}\sum_k a_{j,k_1,k_2}\left(t^{j+1}\right)\varphi_{j,k_1}\left(x_D\right)\varphi_{j,k2}\left(y_D\right) \\ -\sum_k a_{j,k_1,k_2}\left(t^{j}\right)\varphi_{j,k_1}\left(x_D\right)\varphi_{j,k2}\left(y_D\right)\end{array}\right]+\frac{m}{\rho_{sc}\lambda}
\end{aligned} \qquad \text{..... (2.3.6)}$$

Proceeding closely to the process described in the solution of the 1D PDE, the unknown coefficients $\left\{a_{j,k_1,k_2}\right\}$ are obtained using the given/known initial and boundary conditions. These are then used in Eq. (2.3.4) to provide the solution at any desirable point and time in the discretized 2D domain.

2.6 WB Solution of the 3D Equation of Flow

The flow of a nearly incompressible fluid through a 3D homogeneous and isotropic porous medium is described by the following general diffusivity partial differential equation (PDE) already described by Eq. (1.3.4)

$$\frac{\partial^2 p}{\partial x^2}+\frac{\partial^2 p}{\partial y^2}+\frac{\partial^2 p}{\partial z^2}=\frac{\mu\phi c_t}{k_f}\frac{\partial p}{\partial t}+\frac{m}{\rho_{sc}\lambda},\ x\in[0,x_e],y\in[0,y_e],z\in[0,z_e],t\geq 0$$

Normalization of the *x*, *y* and *z* coordinates yields the dimensionless coordinates $x_D=\frac{x}{x_e}$, $y_D=\frac{y}{y_e}$, $z_D=\frac{z}{z_e}$, with. The initial and boundary conditions are defined as:

$$\begin{aligned}
&\frac{\partial p}{\partial x_D}(0,y_D,z_D,t_D)=g_1(y_D,z_D);\quad \frac{\partial p}{\partial x_D}(1,y_D,z_D,t_D)=g_2(y_D,z_D);\\
&\frac{\partial p}{\partial y_D}(x_D,0,z_D,t_D)=g_3(x_D,z_D);\quad \frac{\partial p}{\partial y_D}(x_D,1,z_D,t_D)=g_4(x_D,z_D);\\
&\frac{\partial p}{\partial z_D}(x_D,y_D,0,t_D)=g_5(x_D,y_D);\quad \frac{\partial p}{\partial z_D}(x_D,y_D,1,t_D)=g_6(x_D,y_D);\\
&p(x_D,y_D,z_D,0)=h(t_D)
\end{aligned} \quad \text{..... (2.6.1)}$$

where, $g_i(u,w)$, i = 1, 2, 3, 4, 5, 6 denotes Neumann boundary condition functions, $f(v)$ denotes the initial condition function, and *u*, *v*, and *w* are the general independent variables of the corresponding functions.

Using cubic B-spline bases, the pressure is approximated as:

$$p(x_D,y_D,z_D,t)\approx\sum_k a_{j,k_1,k_2,k_3}(t)\Phi_{j,k_1,k_2,k_3}(x_D,y_D,z_D) \quad \text{..... (2.6.2)}$$

where $\Phi_{j,k_1,k_2,k_3}(x_D, y_D, z_D) = \varphi \otimes \varphi \otimes \varphi(x_D, y_D, z_D) = \varphi_{j,k_1}(x_D)\varphi_{j,k_2}(y_D)\varphi_{j,k_3}(z_D)$, and k_1, k_2, and k_3 are shifting factors of the scaling functions corresponding to the independent variables x_D, y_D and z_D, respectively.

In a manner entirely analogous to that for the solution of the 1D and the 2D PDE, for $(x_D, y_D, z_D) \in (0,1)\times(0,1)\times(0,1)$, the intervals Δx, Δy and Δz between any two successive points on the x-, y- and z-axes, respectively, are defined as:

$$\Delta x = \frac{1}{N_x},\ \Delta y = \frac{1}{N_y},\ \Delta z = \frac{1}{N_z}$$

where N_x, N_y, and N_z denote the number of subdivisions into which the x-, y- and z-axes are discretized. Time is discretized in a manner identical in the 1D and 2D PDE.

Spatial and temporal discretization of Eq. (1.3.4) and substitution of Eq. (2.6.2) using cubic B-spline wavelets yields the WB form of the discretized equation as:

$$\begin{aligned}
&\frac{1}{x_e^2}\sum_k a_{j,k_1,k_2,k_3}\left(t^{j+1}\right)\frac{\partial^2\varphi_{j,k_1}}{\partial x_D^2}(x_D)\varphi_{j,k_2}(y_D)\varphi_{j,k_3}(z_D)\\
&+\frac{1}{y_e^2}\sum_k a_{j,k_1,k_2,k_3}\left(t^{j+1}\right)\varphi_{j,k_1}(x_D)\frac{\partial^2\varphi_{j,k_2}}{\partial y_D^2}(y_D)\varphi_{j,k_3}(z_D)\\
&+\frac{1}{z_e^2}\sum_k a_{j,k_1,k_2,k_3}\left(t^{j+1}\right)\varphi_{j,k_1}(x_D)\varphi_{j,k_2}(y_D)\frac{\partial^2\varphi_{j,k_3}}{\partial z_D^2}(z_D) \qquad \text{..... (2.6.3)}\\
&=\frac{\mu\phi c_t}{\Delta t k_f}\left[\begin{array}{l}\sum_k a_{j,k_1,k_2,k_3}\left(t^{j+1}\right)\varphi_{j,k_1}(x_D)\varphi_{j,k_2}(y_D)\varphi_{j,k_3}(z_D)\\ -\sum_k a_{j,k_1,k_2,k_3}\left(t^{j}\right)\varphi_{j,k_1}(x_D)\varphi_{j,k_2}(y_D)\varphi_{j,k_3}(z_D)\end{array}\right]+\frac{\widehat{m}}{\rho_{sc}\lambda}
\end{aligned}$$

Following the same successive process described in the solution of the 1D and 2D PDEs, the unknown coefficients $\left\{a_{j,k_1,k_2,k_3}\right\}$ at each time step t^{j+1} can be obtained using the known initial and boundary conditions. Next, substitution of the resulting coefficients $\left\{a_{j,k_1,k_2,k_3}\right\}$ into Eq. (2.6.3) yields the pressures at any point and time in the discretized 3D domain.

CHAPTER III

VERIFICATION AND VALIDATION OF THE WB SOLUTION OF THE PDE OF FLOW

In this chapter, several examples of the WB solutions of PDEs for flow through porous media are investigated in order to:

- Compare the WB numerical solutions to existing analytical solutions in a one-dimensional space.
- Contrast the explicit method with the implicit WB numerical method.
- Compare the errors of the WB solutions obtained using the Haar and the B-spline wavelets.
- Compare WB numerical solutions to results obtained from the FTSim (Wang, 2019) numerical simulator in a multidimensional space.

3.1 Case 1: 1D Flow, Cartesian Domain, Constant Production Rate, Constant-Pressure (Dirichlet) boundary

For a constant pressure at the outer boundary, an analytical solution to the dimensionless diffusivity equation of flow through a porous medium in a 1D domain — Eqs. (1.3.6), (2.4.5) and (2.4.6) — in the Laplace domain was provided by Blasingame (1996) as:

$$\overline{p_D} = \frac{1}{s\sqrt{s}} \frac{\sinh\left[\sqrt{s}\left(1-x_D\right)\right]}{\cosh\left(\sqrt{s}\right)} \quad \text{.....} (3.1.1)$$

where, $\overline{p_D}(s) = \mathcal{L}\{p_D(t)\}$, L{} denotes the Laplace transform of the quantity within the brackets, and *s* is the Laplace parameter.

The Stehfest algorithm (1970) was applied to numerically invert the Laplace domain solution described by Eq. (3.1.2) in order to obtain the solution in time. Per the suggestions of Moridis and Reddell (1991) and Moridis *et al.*. (1999, 2021), the number of terms used in the series of the Stehfest algorithm is 18 for all cases.

The WB numerical solution used the cubic B-spline wavelet (m = 4) and set the resolution level j = 4. The dimensionless spatial domain is $x_D \in [0,1]$, and the dimensionless time domain is $t_D \in [0,5]$. The time interval is $\Delta t = 10^{-4}$. Two x_D discretizations were used. In the first, the space interval $\Delta x_1 = 0.01$, and in the second the space interval $\Delta x_2 = 0.01$. The simulation was conducted following the equations and derivations discussed in **Section 2.4.2**.

Fig. 3.1 shows an excellent agreement between the analytical and the WB solutions of the evolution of the p_D over t_D as a function of x_D. This is confirmed by **Fig. 3.2**, which presents the deviation — referred to as "error" when the analytical solution is taken as the reference solution — between the analytical and the WB numerical solution with regard to dimensionless time and distance. The absolute error shown in **Fig. 3.2** is computed as follows:

$$\varepsilon_i = \left| p_i^{analytical} - p_i^{numerical} \right| \quad \text{..... (3.1.2)}$$

where ε is the absolute error.

The maximum deviation between the two solutions is on the order of 10^{-4} and is observed early in the course of production. For $t_D > 1$, the deviations between the two solutions are

consistently on the order of 10^{-5} or lower, thus providing evidence in support of the validity and accuracy of the WB numerical solution.

In addition, in order to provide another quantitative measure of the accuracy and overall performance of the WB numerical solution, we computed the error norms L_2 and L_∞ against the analytical solutions.

$$L_2 = \sqrt{\Delta x \sum_i \left| p_i^{analytical} - p_i^{numerical} \right|^2} \quad \text{..... (3.1.3)}$$
$$L_\infty = \max_i \left| p_i^{analytical} - p_i^{numerical} \right|$$

The results for the two different Δx discretizations appear in **Table 3.1** and show a clear dependence of the error on the Δx size; as expected, both L_2 and $L\infty$ decrease consistently with a decreasing Δx. However, the WB numerical solution is shown to be highly accurate even for the relatively coarse discretization bases on the larger $\Delta x = 0.01$.

Table 3.1 – Case 1: comparison of the error norms.

Cubic B-spline Wavelets		$\Delta x = 0.01$	$\Delta x = 0.005$
$x_D = 0$	L_2	1.39E-06	8.61E-07
	L_∞	1.04E-04	1.26E-04
$x_D = 0.25$	L_2	1.28E-06	7.41E-07
	L_∞	9.61E-05	1.07E-04
$x_D = 0.5$	L_2	1.02E-06	5.57E-07
	L_∞	7.78E-05	7.97E-05
$x_D = 0.75$	L_2	5.71E-07	3.01E-07
	L_∞	4.39E-05	4.29E-05

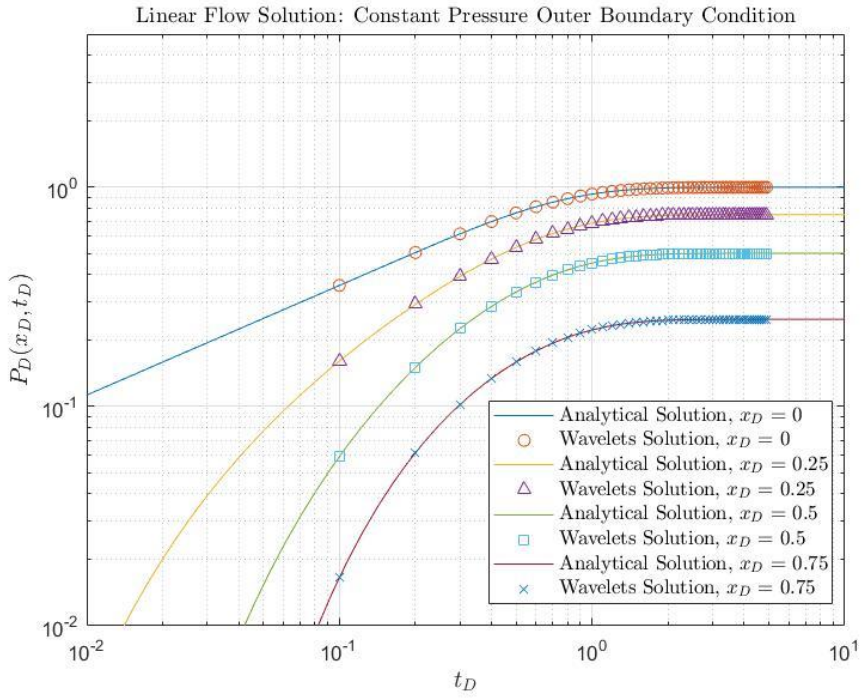

Figure 3.1 – Comparison of (a) the analytical and (b) the WB numerical solution using cubic B-spline wavelet bases for $\Delta x = 0.005$ in **Case 1**: Reservoir pressure p_D as a function of t_D and x_D.

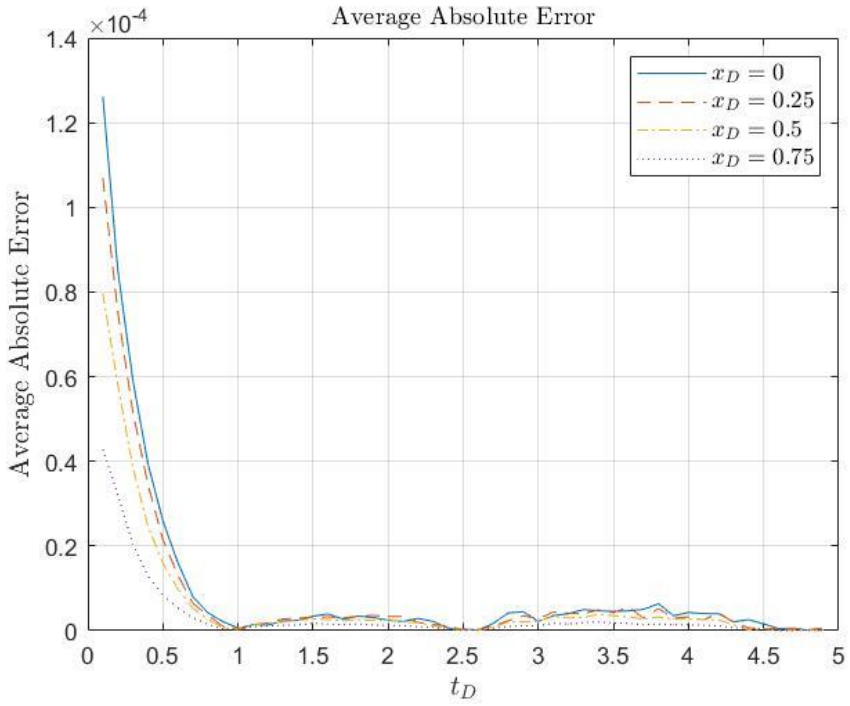

Figure 3.2 – Case 1: Absolute deviation between the analytical (reference) solution and the WB numerical solutions using cubic B-spline wavelet bases for Δx = 0.005 as a function of t_D and x_D.

3.2 Case 2: 1D Flow, Cartesian Domain, Constant Production Rate, No Flow (**Neumann boundary conditions**)

For a no flow outer boundary condition, an analytical solution to the dimensionless diffusivity equation of flow through a porous medium in a 1D domain — Eqs. (1.3.6), (2.4.5) and (3.2.1):

$$\frac{\partial p_D}{\partial x_D}\left(x_D = 1, t_D\right) = 0 \quad \text{..... (3.2.1)}$$

Blasingame (1996) proposed the following analytical solution to this problem in the Laplace domain:

$$\overline{p_D} = \frac{1}{s\sqrt{s}} \frac{\cosh\left[\sqrt{s}\left(1-x_D\right)\right]}{\sinh\left(\sqrt{s}\right)} \quad \text{..... (3.2.2)}$$

The WB numerical simulation in Case 2 also used cubic B-spline wavelets (m = 4). Time and space are discretized in a manner identical to that in **Case 1**. The WB simulation was conducted following the derivations in **Section 2.4.2**.

For this case, the Stehfest algorithm (1970) was applied to numerically invert the Laplace space solution described by Eq. (3.2.2). The number of terms in the Stehfest algorithm series is 18 for all cases.

The analytical and the WB solutions of the evolution of p_D over t_D as a function of x_D are shown in **Fig. 3.3** and show a very good agreement. The deviation of the WB solution from the baseline (reference) analytical solution is deemed as an "error" and is shown in **Fig 3.4** for $\Delta x = 0.01$. The absolute error that is depicted in **Fig. 3.4** is computed by Eq. (3.1.3)

Note that, unlike the observations in **Fig. 3.2**, the (obviously small) errors in **Fig. 3.4** appear to increase with t_D for any x_D and are consistently and significantly larger (by 2-3 orders of magnitude) than those of **Fig. 3.2**. This is confirmed by the estimates of the error norms in **Table 3.2**, all of which are on the order of 10^{-6} – 10^{-5} and are more than plain satisfactory.

Table 3.2 – Case 2: comparison of the error norms

Cubic B-spline Wavelets		$\Delta x = 0.01$	$\Delta x = 0.005$
$x_D = 0$	L_2	5.55E-06	2.95E-06
	L_∞	1.04E-04	1.26E-04
$x_D = 0.25$	L_2	5.53E-06	2.92E-06
	L_∞	9.65E-05	1.07E-04
$x_D = 0.5$	L_2	5.52E-06	2.90E-06
	L_∞	8.16E-05	8.41E-05
$x_D = 0.75$	L_2	5.49E-06	2.87E-06
	L_∞	8.17E-05	8.36E-05

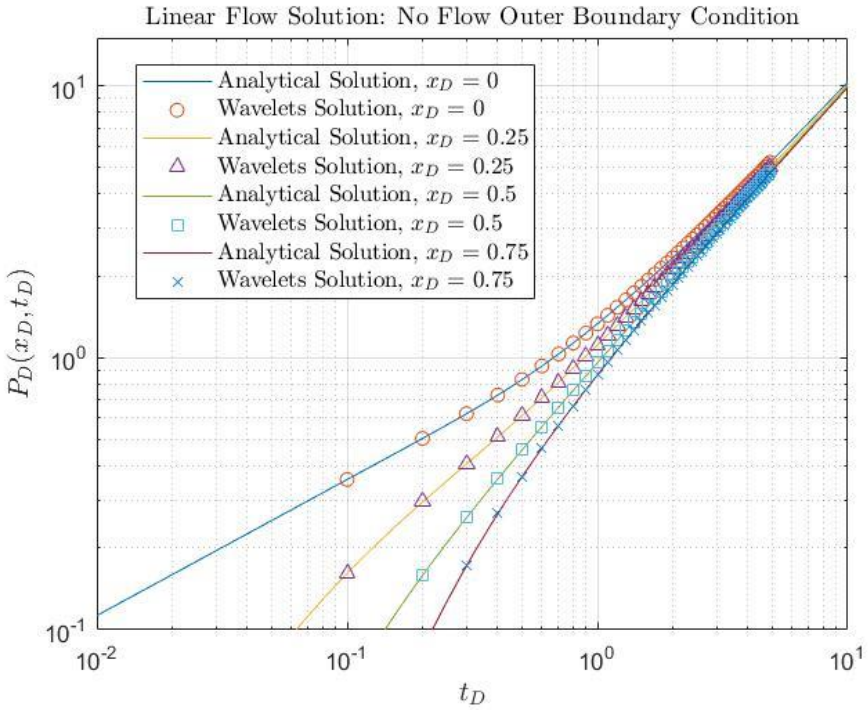

Figure 3.3 – Comparison of the analytical and the WB numerical solution using cubic B-spline wavelet bases for $\Delta x = 0.005$ in **Case 2**: Reservoir pressure p_D as a function of t_D and x_D

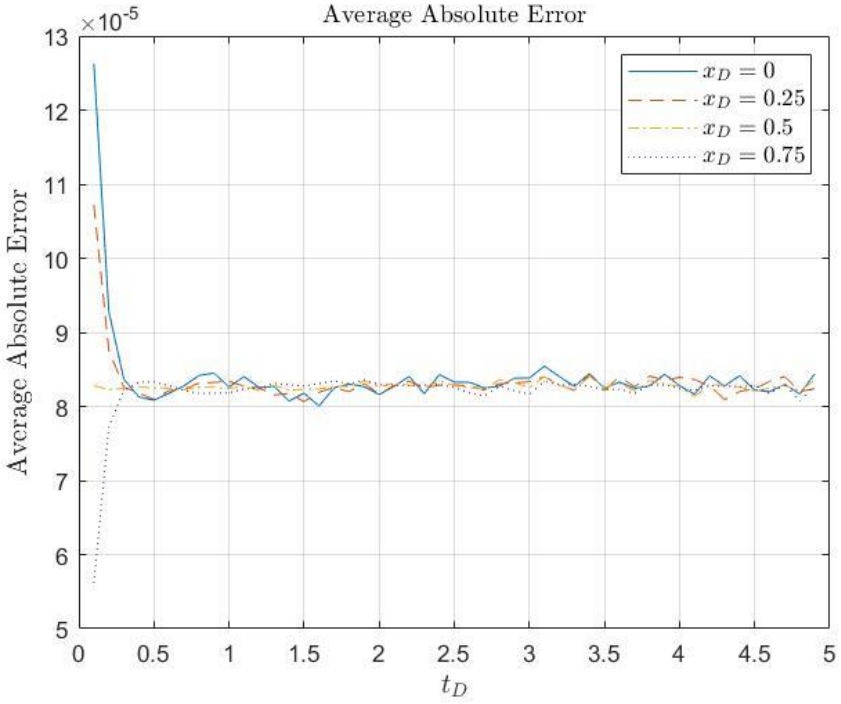

Figure 3.4 – **Case 2**: Absolute deviation between the analytical (reference) solution and the WB numerical solutions using cubic B-spline wavelet bases for Δx = 0.005 as a function of t_D and x_D.

3.3 Case 3: Comparative Evaluation of the Performance of WB Solutions using Haar and B-spline Wavelets

This study investigates the differences in the performance of the WB numerical solution caused by the use of two-different types of wavelets: Haar and B-splines. The problem chosen for this study is the one discussed in **Case 1** involving 1D flow through a porous medium in response to a constant-rate production from a domain with constant-pressure conditions at its outer boundary.

The difference between the implementation of the Haar and the B-spline wavelets is that the former involve integration, which has been demonstrated in Eqs. (2.4.10) and (2.4.11)

in **Section 2.4.1**, while the latter involve differentiation, which has been stated in Eq. (2.4.17) in **Section 2.4.2**. The performance of the WB numerical solution using B-spline (cubic) wavelets has already been discussed in **Case 1** and is described in **Table 3.1** and **Figs. 3.1** and **3.2**.

The WB solutions of the evolution of p_D vs. t_D for various x_D using the Haar wavelets are shown in **Fig. 3.5**, and the deviation between the Haar WB solutions and the analytical solutions (considered the reference and correct solution) are shown in **Fig. 3.6**. The deviation, namely the absolute error, is calculated by Eq. (3.1.3)

The analytical solution is also obtained from Eq. (3.1.2) using the Stehfest algorithm to obtain the solution in the real-time domain. The procedures and parameters of the numerical inversion are identical to those in **Case 1**.

The WB numerical solution involved Haar wavelets and a resolution level $j = 5$. The dimensionless spatial domain is $x_D \in [0,1]$ and the dimensionless time domain is $t_D \in [0,10]$. The time interval is $\Delta t = 10^{-5}$ and the space interval is $\Delta x = 1/2^6$. The whole simulation was conducted following the derivations in **Section 2.4.1**.

Comparison to the results of the WB numerical solution in **Case 1** (**Fig. 3.1,** and **3.2**) provides clear evidence of the superiority of B-spline wavelets; the deviations between the analytical solutions and the Haar wavelet-based predictions are in the order of 10^{-3} to 10^{-1}, *i.e.*, still satisfactory, but about 2 to 3 orders of magnitude higher than those of the WB solutions for B-spline wavelets.

The reason for the superiority of the B-spline wavelets may be the shape of those two wavelet bases. Haar wavelets have shapes defined by two straight lines that form rectangular footprints; on the other hand, B-spline wavelets involve smooth curves that, intuitively, are expected to be easier to conform to the shape of a changing function.

The conclusion to be drawn from this study is that B-spline wavelets are more appropriate bases in the WB numerical solution of PDEs, yielding more accurate solutions. Therefore, only B-spline wavelets are used as the bases for all subsequent WB numerical studies.

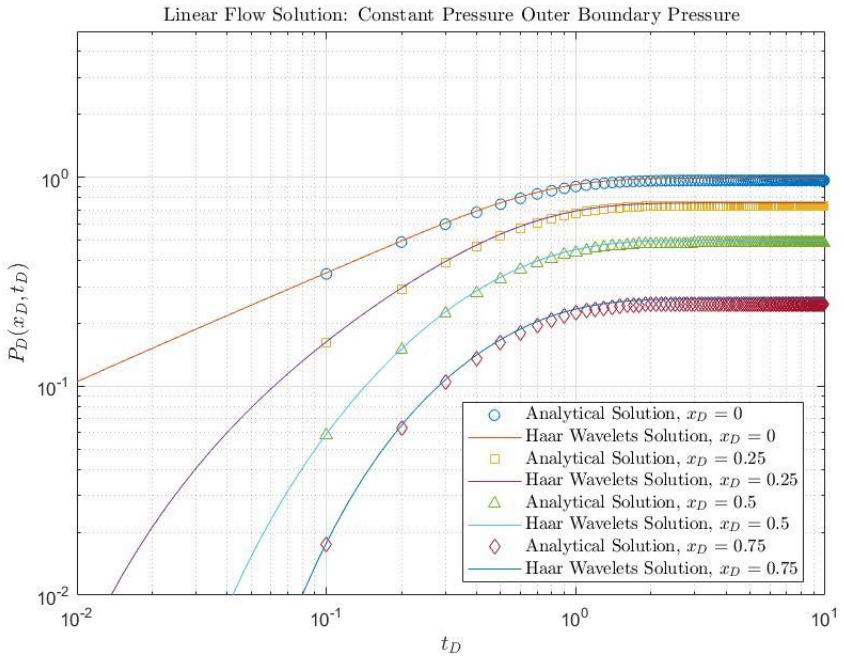

Figure 3.5 – Comparison of the analytical and the WB numerical solution using Haar wavelet bases in **Case 3**: Reservoir pressure p_D as a function of t_D and x_D**.**

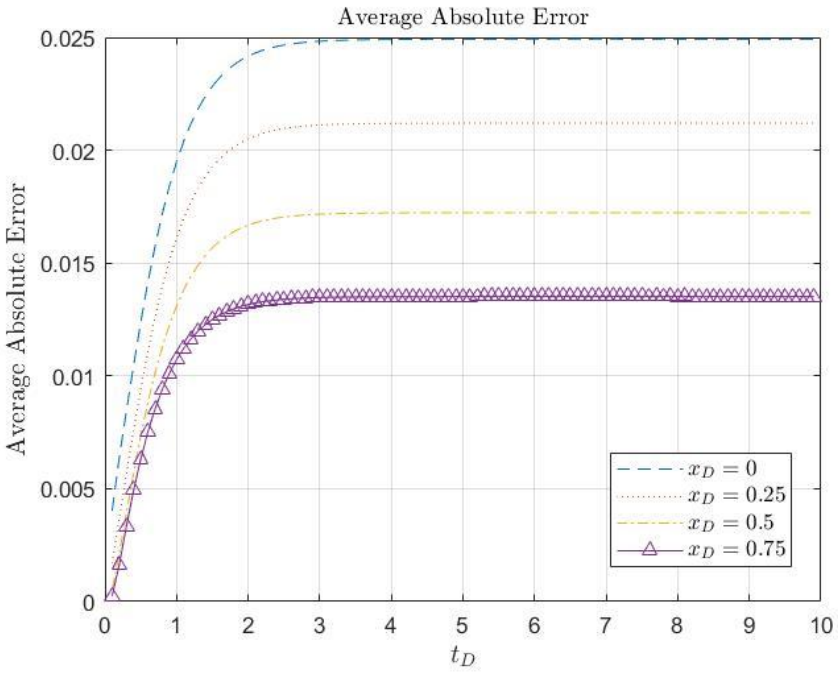

Figure 3.6 – Case 3: Absolute deviation between the analytical (reference) solution and the WB numerical solutions using Haar wavelet bases for $\Delta x = 1/2^6$ as a function of t_D and x_D.

3.4 Case 4: 2D Flow, Cartesian Domain, Constant Production Rate, No Flow (**Neumann**) **boundary**

The **Case 4** is an application problem designed to show the validity of the WB numerical solution to a 2D problem flow for which there is no analytical solution. The general 2D equation of flow through a homogeneous and isotropic porous medium in an aerial system (*i.e.*, involving a single layer in the vertical direction describing the reservoir thickness) have already been described by Eqs. (2.3.3) and (2.3.4).

Evidence in support of the validity of the WB solution is provided through comparison to results obtained from the FTSim numerical simulator (Wang, 2019). In this case, the well that is producing at a constant rate is located at the center of the domain (see **Fig. 3.7**).

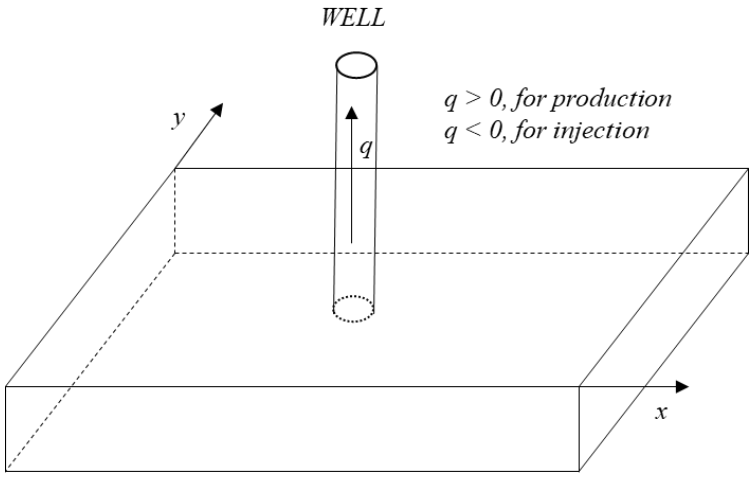

Figure 3.7 – Case 4: Sketch of the 2D domain

The parameters used in the numerical simulation are listed in **Table 3.3**. The spatial discretization of the domain for the WB solution is 1 meter × 1 meter. I used a resolution level $j = 4$, and the order m of the B-spline wavelets is 4 as well. The numerical computing followed the derivations in **Section 2.5**. The spatial discretization of the domain for the FTSim solution is also 1 meter × 1 meter.

The WB prediction and FTSim solution of the reservoir pressure on the y-plane at $x = 25.5$ m in the 2D reservoir at $t = 0.1$-day, 1 day, 2days, 10 days, 1 month, 2 months, 3 months and 4 months are shown in **Figs. 3.8** and **3.9**. The deviations between the two solutions, namely the relative error η, is computed using the following equation.

$$\eta_i = \frac{\left| p_i^{FT-Sim} - p_i^{WB} \right|}{p_i^{FT-Sim}} \quad \text{..... (3.4.2)}$$

The average η between the FTSim and WB results is on the order of 10^{-4} and the maximum discrepancies between the two solutions are observed at the location/element of the production well. However, even these (and all the smaller discrepancies) are around 0.023%, which indicates an excellent match of two sets of solutions and provides further evidence in support of validation of the WB numerical method.

Table 3.3 – Case 4: Input Parameters for WB and FTSim Simulations

Parameter	Value
Order of B-spline wavelets *m*	4
Level of resolution *J*	4
Production rate *q*	0.01 kg/s
Initial pressure p_i	3×10^7 Pa
Porosity φ	0.25
Oil compressibility, c_o	5×10^{-9} Pa^{-1}
Oi density, ρ	811.39 kg/m^3
Oil viscosity, μ	3.11×10^{-4} Pa·s
Formation permeability, k_f	2.5×10^{-13} m^2
Rock compressibility, c_r	1×10^{-9} Pa^{-1}
Domain length *x*	51 m
Domain width *y*	51 m
Domain depth *z*	20 m

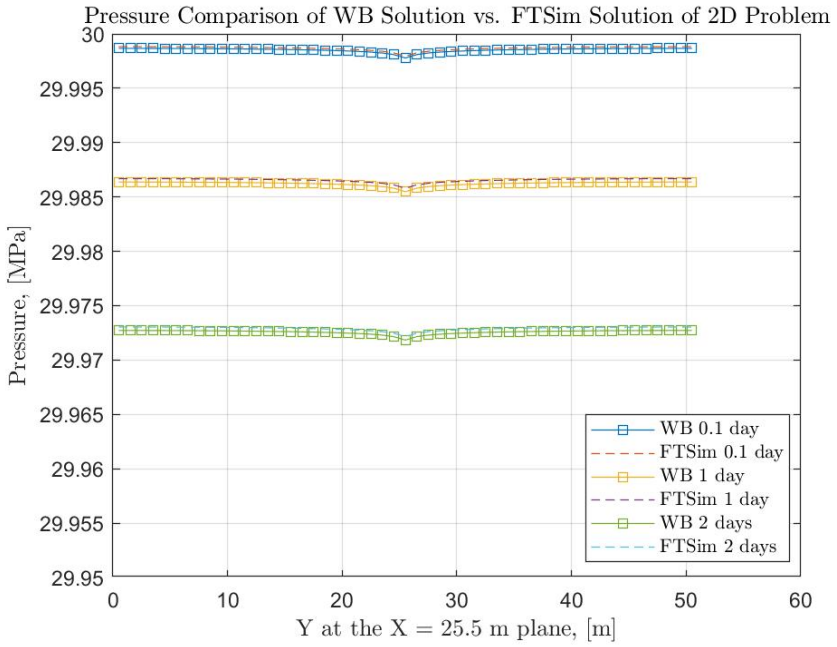

Figure 3.8 – Case 4: Evolution of pressure distribution over time between the WB and the FTSim solutions in the y-direction at x = 25.5 m for constant-rate production.

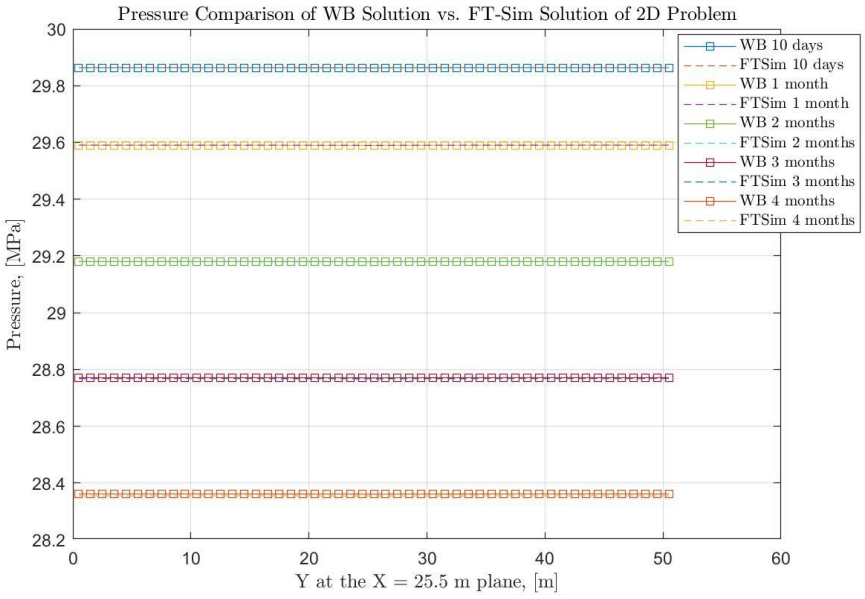

Figure 3.9 – Case 4: Evolution of pressure distribution over time between the WB and the FTSim solutions in the y-direction at x = 25.5 m for constant-rate production.

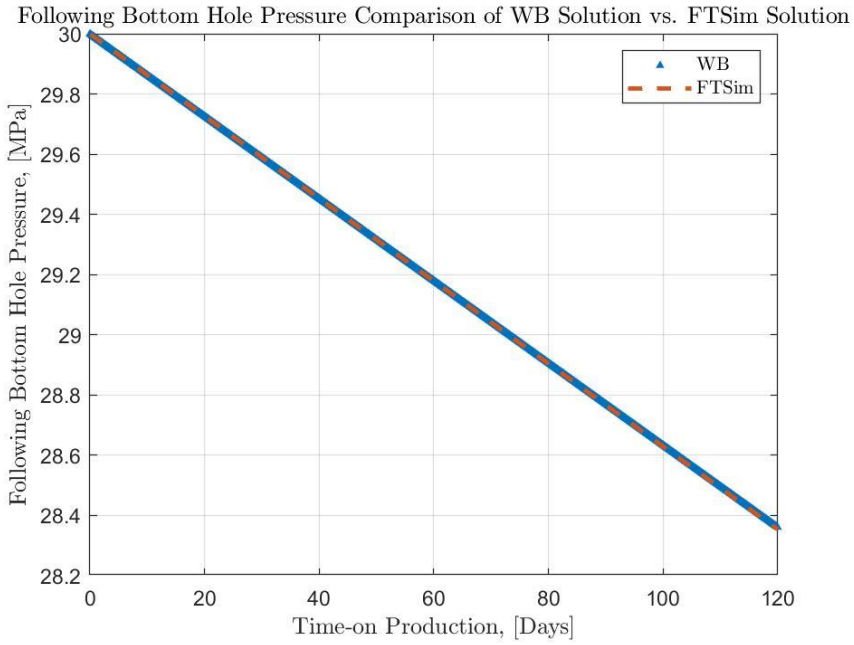

Figure 3.10 – Case 4: Evolution of following bottom hole pressure over time the WB and the FTSim solutions in the y-direction at x = 25.5 m and y = 25.5 m for constant-rate production.

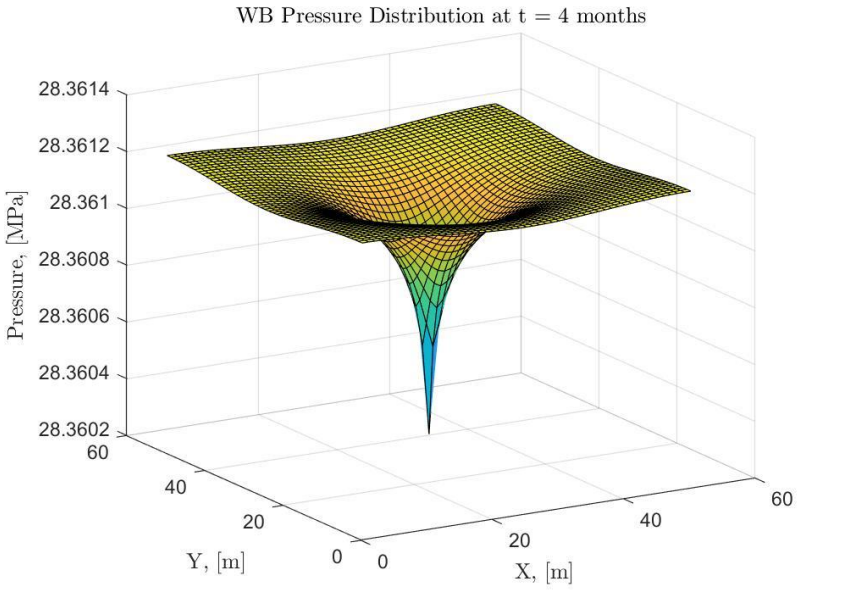

Figure 3.11 – Case 4: Reservoir pressure distribution of the WB pressure results in the 2D domain at t = 4 months for constant-rate production.

3.5 Case 5: 3D Flow, Cartesian Domain, Constant Production Rate, No Flow (**Neumann**) **boundary**

As in **Case 4**, this is an application problem designed to show the validity of the WB numerical solution to a 3D problem flow for which there is *no analytical solution*. This problem is described by the general 3D equation of Eq. (1.3.4) as

$$\frac{\partial^2 p}{\partial x^2}+\frac{\partial^2 p}{\partial y^2}+\frac{\partial^2 p}{\partial z^2}=\frac{\mu\phi c_t}{k}\frac{\partial p}{\partial t}+\frac{m}{\rho_{sc}\lambda}$$

Eq. (2.6.1) is rewritten in terms of the volumetric production rate q instead of the mass production rate m:

$$\frac{\partial^2 p}{\partial x^2}+\frac{\partial^2 p}{\partial y^2}+\frac{\partial^2 p}{\partial z^2}=\frac{\mu\phi c_t}{k}\frac{\partial p}{\partial t}+\frac{q}{\rho_{sc}\lambda V_0} \quad \text{..... (3.3.1)}$$

The above parameters are defined as in **Case 4**.

As in **Case 4**, the validity of the WB solution will be provided through its comparison to the results from the FTSim numerical simulator (Wang, 2021). A description of the domain is provided in the sketch of **Fig. 3.10**, which also shows the reservoir dimensions and the well that is located at the center of the domain and is producing at a constant rate. The well is completed in the entire length of the reservoir thickness in the *z*-direction. Detailed information on the reservoir properties, the initial conditions, and the domain dimensions are described in **Table 3.4.**

The spatial discretization of the domain for the WB solution is 1 meter × 1 meter × 1 meter. A resolution level $j = 4$ is used, and the order m of the B-spline wavelets is 4 as

well. The numerical computations followed the equations and derivations in **Section 2.6**. The spatial discretization of the domain for the FTSim solution is also 1 meter × 1 meter × 1 meter.

The WB prediction and the FTSim solution of the pressure along the *y*-plane at x = 5.5 m and z = -4.5 m in the 3D reservoir at t = 1 day, 10 days, 30 days, 60 days are shown in **Fig. 3.13**. The average deviation, defined in Eq. (3.4.2), between WB and the FTSim results is around 0.3%. This provides evidence of the validity and accuracy of the WB solutions.

Table 3.4 – Case 5: Input Parameters for WB and FTSim Simulations

Parameter	**Value**
Order of B-spline wavelets m	4
Level of resolution J	4
Production rate q	1×10^{-3} kg/s
Initial pressure p_i	3×10^{7} Pa
Porosity φ	0.25
Oil compressibility, c_o	5×10^{-9} Pa^{-1}
Oi density, ρ	811.39 kg/m^3
Oil viscosity, μ	3.11×10^{-4} Pa·s
Formation permeability, k_f	2.5×10^{-13} m^2
Rock compressibility, c_r	1×10^{-9} Pa^{-1}
Domain length x	11 m
Domain width y	11 m
Domain depth z	5 m

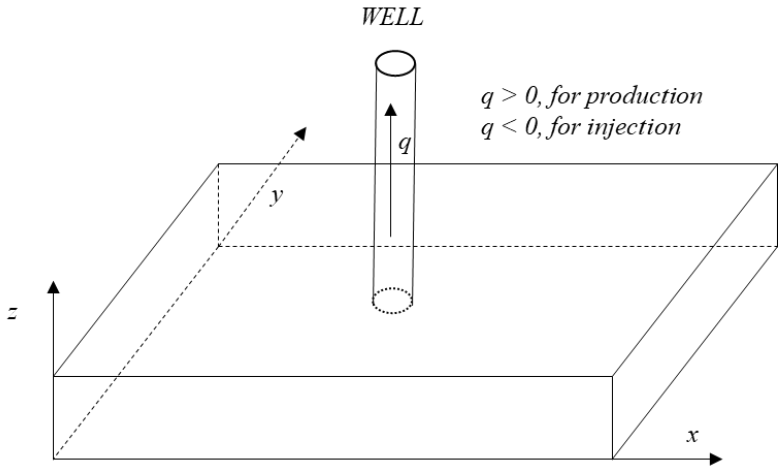

Figure 3.12 – Case 5: Sketch of the 3D domain.

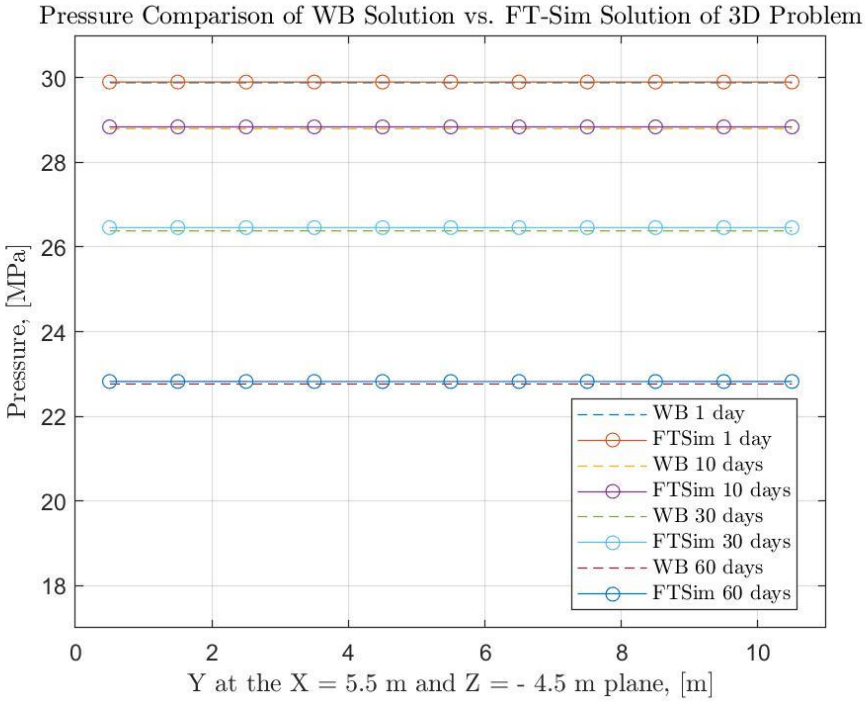

Figure 3.13 – Case 5: Evolution of pressure distribution over time between the WB and the FTSim solutions in the y-direction at x = 5.5 m and z = -4.5 m for constant-rate production.

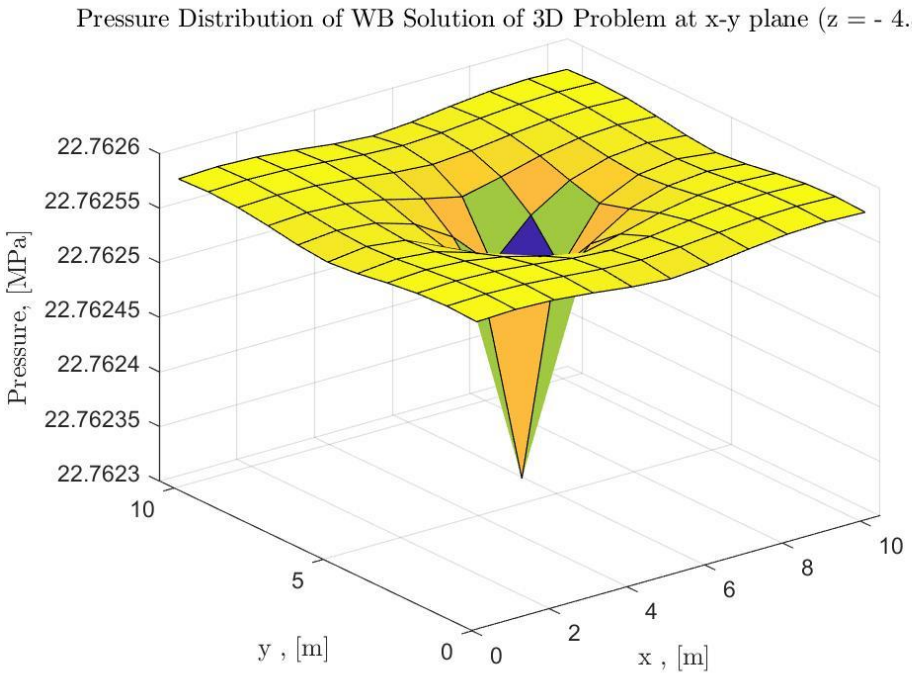

Figure 3.14 – Case 5: Reservoir pressure distribution of WB results in the 3D domain at t = 60 days for constant-rate production

3.6 Case 6: 1D Two-Phase Flow, Cartesian Domain, Constant-water saturation (**Dirichlet boundary conditions**)

The Buckley-Leverett two-phase flow model neglects gravitational force and capillary pressure and assumes that (a) the fluids are immiscible and incompressible and that (b) the porous medium is homogeneous. The related PDE is given as follows:

$$\frac{\partial S_w}{\partial t} = -\frac{q}{\phi A}\frac{\partial f_w(S_w)}{\partial x} \quad \text{..... (3.6.1)}$$

where S_w is the water saturation, f_w is the fractional flow of water defined in Eq. (3.6.2), q is the constant volumetric injection/production rate, and the other terms are as defined in **Section 1.3**. Additionally,

$$f_w = \begin{cases} 0, & \text{if } 0 < S \le S_{wr} \\ \dfrac{\lambda_w}{\lambda_w + \lambda_o}, & \text{if } S_{wr} < S \le 1 - S_{or} \\ 1, & \text{if } 1 - S_{or} < S \le 1 \end{cases} \quad \text{..... (3.6.2)}$$

The terms λ_w and λ_o are the water and oil mobilities, respectively, that are defined as

$$\lambda_w = \left(S_w - S_{wr}\right)^2, \ \lambda_o = \left(1 - S_w - S_{or}\right)^2 \quad \text{..... (3.6.3)}$$

where S_{wr} and S_{or} are the water and oil irreducible saturations, respectively.

The initial and boundary conditions are:

$$S_w\left(x = 0, t\right) = 1 - S_{or}, \ S_w\left(x, t = 0\right) = S_{wr} \quad \text{..... (3.6.4)}$$

Both linear and cubic B-spline wavelets are used in the solution of the 1D two-phase flow problem. As in Eq. (2.4.1), the water saturation can be approximated as follows.

$$S_w\left(x,t\right) \approx \sum_{i=1}^{\infty} a_{j,k}\left(t\right)\varphi_{j,k}\left(x\right) \quad \text{..... (3.6.4)}$$

The procedure to discretize Eq. (3.6.1) and substitute Eq. (3.6.4) is like that in Eqs. (2.4.16) to (2.4.18), yielding the expression:

$$\sum_{i=1}^{\infty} a_{j,k}\left(t^{s+1}\right)\varphi_{j,k}\left(x^l\right) = \sum_{i=1}^{\infty} a_{j,k}\left(t^s\right)\varphi_{j,k}\left(x^l\right) - \frac{q\Delta t}{\phi A \Delta x}\left[f_w\left(x^l, t^s\right) - f_w\left(x^{l-1}, t^s\right)\right] \quad \text{..... (3.6.5)}$$

For the WB numerical simulation, the spatial domain is $x \in [0,1]$, and the time domain is $t \in [0,1500]$ [days]. The time interval is Δt = 37.5 [days], and the space interval is $\Delta x = \frac{1}{n_p}$, where n_p is the number of collocation points, defined by the relationship $n_p = 2^j + m - 1$.

The comparisons of the WB numerical solution to both the analytical solution and the numerical solution from the finite difference (FD) method are shown in **Figs. 3.13** to **3.18**. Evidently, as the resolution level *j* increases, the accuracy of the solution increases. For a resolution level j = 6, the WB solution is in excellent agreement with the analytical solution. Similarly, as the B-spline order *m* increases from 2 to 4, the accuracy of the solution also increases. Note that the B-spline order *m* has a smaller impact on the accuracy of the solutions than the resolution level, and the improvement in the accuracy of the WB solutions with an increasing order of the splines is more obvious at the lower resolution level (j = 4).

Table 3.5 – Case 6: Input Parameters for WB Simulation

Parameter	Value
Order of B-spline wavelets *m*	2, 4
Level of resolution *J*	4, 5, 6
Injection/Production rate q	0.5335×10^{-4} m/s
Cross-section area *A*	1 m^2
Porosity φ	0.25
Oil irreducible saturations, S_{or}	0.2
Water irreducible saturations, S_{wr}	0.16
Domain length *x*	1 m

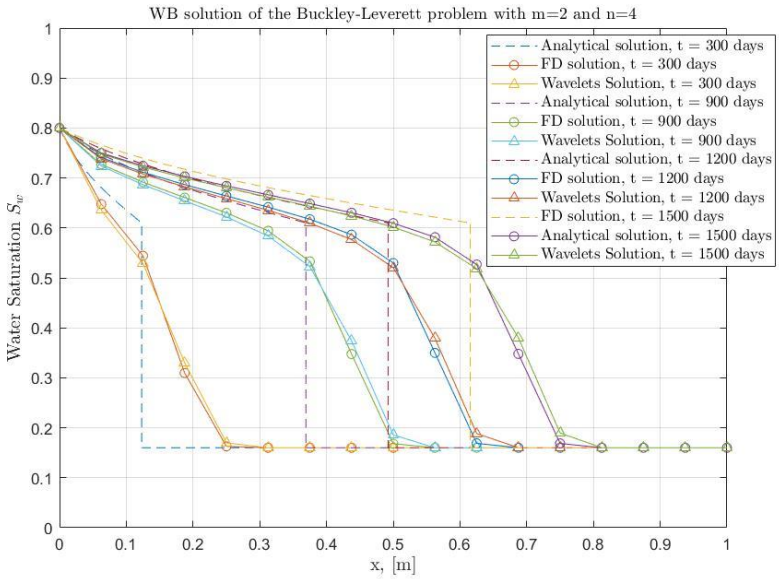

Figure 3.15 – Case 6: Water saturation S_w distribution over time in the *x*-direction for the Buckley-Leverett problem: comparison of the WB solution (m = 2, n = 4), the FD solution and the analytical solution.

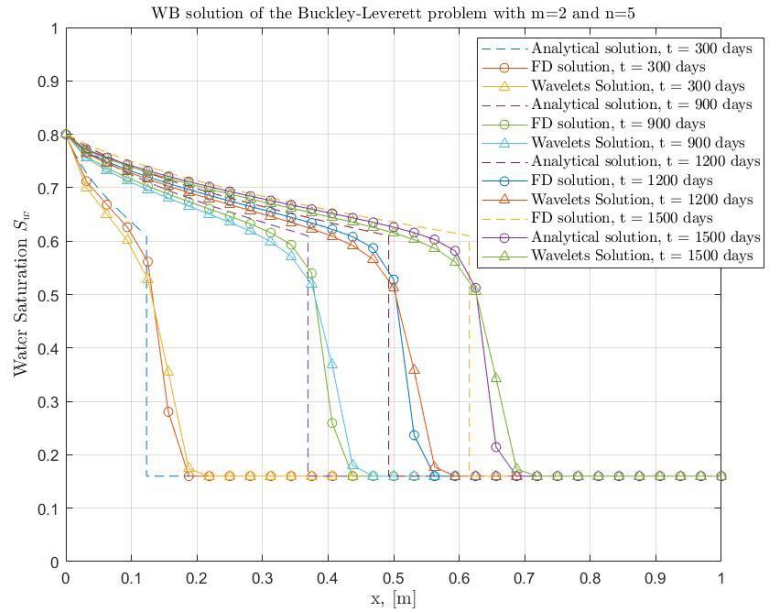

Figure 3.16 – Case 6: Water saturation S_w distribution over time in the *x*-direction for the Buckley-Leverett problem: comparison of the WB solution (m = 2, n = 5), the FD solution and the analytical solution..

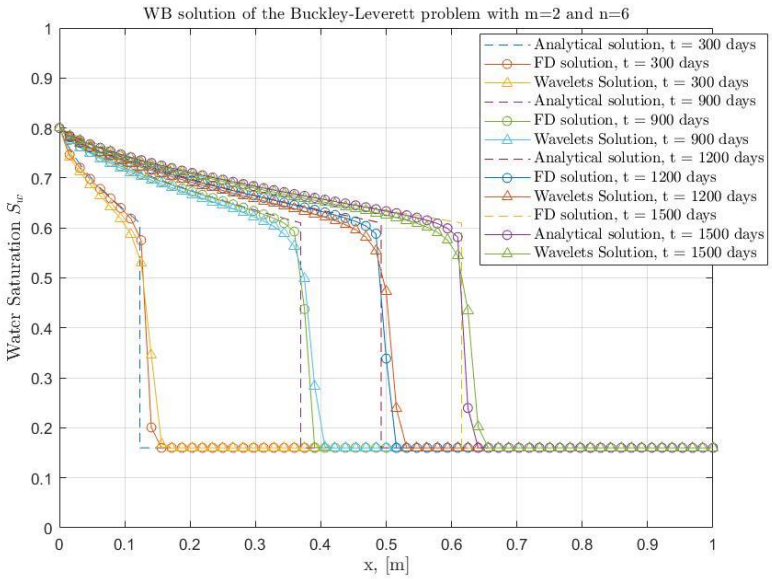

Figure 3.17 – Case 6: Water saturation S_w distribution over time in the *x*-direction for the Buckley-Leverett problem: comparison of the WB solution (m = 2, n = 6), the FD solution and the analytical solution.

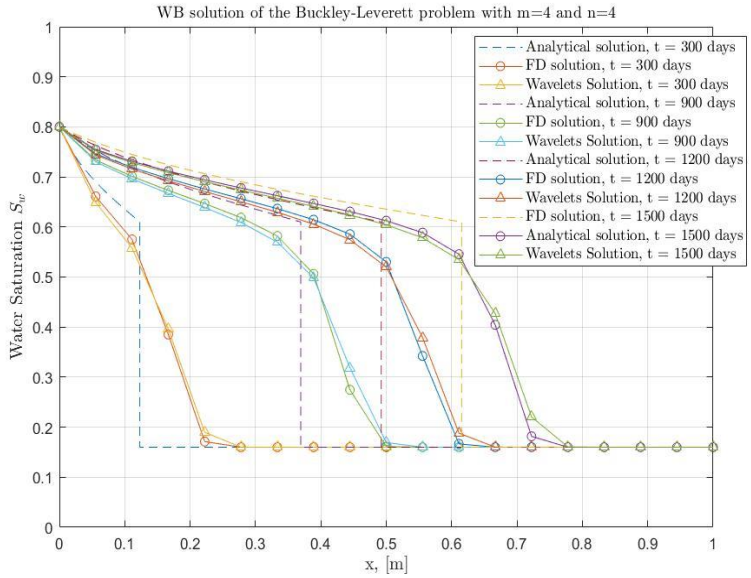

Figure 3.18 – Case 6: Water saturation S_w distribution over time in the *x*-direction for the Buckley-Leverett problem: comparison of the WB solution (m = 4, n = 4), the FD solution and the analytical solution.

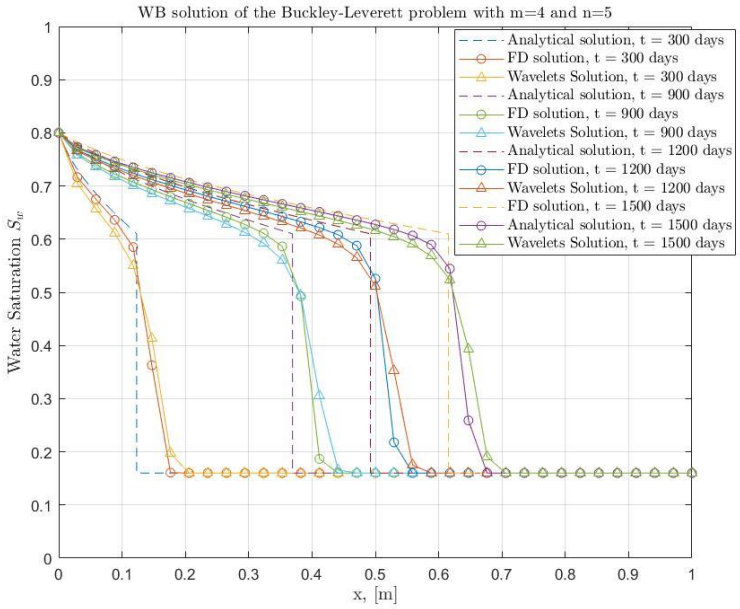

Figure 3.19 – Case 6: Water saturation S_w distribution over time in the *x*-direction for the Buckley-Leverett problem: comparison of the WB solution (m = 4, n = 5), the FD solution and the analytical solution.

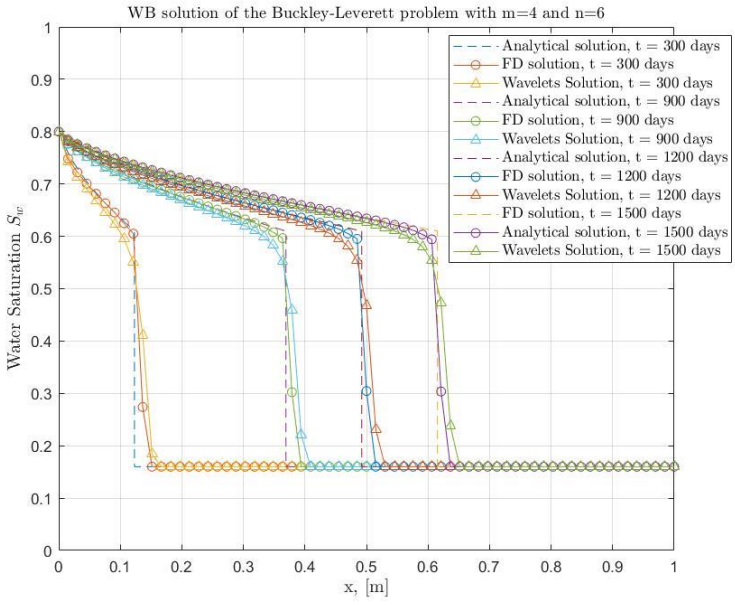

Figure 3.20 – Case 6: Water saturation S_w distribution over time in the *x*-direction for the Buckley-Leverett problem: comparison of the WB solution (m = 4, n = 6), the FD solution and the analytical solution.

3.7 Case 7: Evaluation of the Performance of WB Solutions Applying Multiresolution Properties with B-spline Wavelets

In this section, Mallat's decomposition and reconstruction algorithms (1989) are combined based on wavelets and the two-scale method (Daubechies, 1991; Nikolaou and Yong, 1994) to evaluate the performance of WB solutions.

According to Mallat (1989), the relationship between coefficients obtained from difference resolution levels $\{a_{j,k}\}$ and $\{a_{j+1,k}\}$ only depends on the wavelet basis itself. Recalling the subspace V_j from **Section** 2.1, the set of scaling functions $\{\varphi_{j,k}\}$ form a Riesz basis of this space, and defining another subspace W_j yields:

$$V_{j+1} = V_j \oplus W_j \quad \text{..... (3.7.1)}$$

where the subspace W_j is the orthogonal complement of V_j to V_{j+1}.

After defining two operators $A_j : f(x) \in L^2(\mathbb{R})$ where $A_j f(x) \in V_j$ and $D_j : f(x) \in L^2(\mathbb{R})$ where $D_j f(x) \in W_j$, we can approximate the functions as follows.

$$A_j f(x) = \sum_k a_{j,k} \varphi_{j,k}(x) \quad \text{..... (3.7.2)}$$

$$D_j f(x) = \sum_k b_{j,k} \psi_{j,k}(x) \quad \text{..... (3.7.3)}$$

Therefore, the function $f(x)$ can be decomposed as follows (Moridis et al., 1996).

$$A_j p(x) = \sum_k a_{j,k} \varphi_{j,k}(x) = \underbrace{\sum_k a_{j-1,k} \varphi_{j-1,k}(x)}_{A_{j-1} p(x) \in V_{j-1}} + \underbrace{\sum_k b_{j-1,k} \psi_{j,k}(x)}_{D_{j-1} p(x) \in W_{j-1}} \quad \text{..... (3.7.4)}$$

The efficient decomposition algorithm is stated as follows (Mallat, 1989).

$$\begin{pmatrix} a \\ b \end{pmatrix}_{j,l} = \frac{1}{2}\begin{pmatrix} g(l-2k) \\ h(l-2k) \end{pmatrix} a_{j+1,k} \quad \text{..... (3.7.5)}$$

Similarly, the reconstruction algorithm (Mallat, 1989):

$$a_{j+1,l} = \sum_k \left[p(l-2k)\, a_{j,k} + q(l-2k)\, b_{j,k} \right] \quad \text{..... (3.7.6)}$$

The $g(k)$ and $h(k)$ are called decomposition sequences, the $p(k)$ and $q(k)$ are called reconstruction sequences, and they only depend on the wavelet basis itself.

Considering a linear differential equation:

$$L\left[p(x) \right] = f(x) \quad \text{..... (3.7.7)}$$

where L is a linear differential operator.

Substituting the wavelet series representation of the pressure function $p(x)$ as Eq. (2.4.15) in Eq. (3.7.7) and rearrange to the residual expression at resolution level j:

$$R_j(x) = L\left[p_j(x) \right] - f(x) \quad \text{..... (3.7.8)}$$

By solving Eq. (3.7.8), we obtain a set of wavelet coefficients and an approximate solution at resolution level j. However, if the residual is unsatisfactory at this resolution level, we can apply Eq. (3.7.4) to go up to the next resolution level $j+1$:

$$R_{j+1}(x) = L\left[p_{j+1}(x) \right] - f(x) \quad \text{..... (3.7.9)}$$

where $L\left[p_{j+1}(x) \right] = L\left[A_{j-1} p_j(x) + D_{j-1} p_j(x) \right]$.

Therefore, we can solve for the set of wavelet coefficients $\{b_{j,k}\}$ and obtain the pressure function at a higher resolution level $j+1$ through the reconstruction algorithm.

I investigate the above-stated WB numerical method on the **Case 1** involving 1D flow through a porous medium with a constant-rate production from a domain with constant-pressure conditions at its outer boundary as demonstrated in Eqs. (1.3.6), (2.4.5) and (2.4.6). The reconstructed WB results from **Figs. 3.20-3.22** are compared against analytical solution as stated in Eq (3.1.1) for different reconstructed resolution levels j from 2 to 4.

The agreement between two solutions is getting better when we reconstruct the solution from a lower resolution level to a higher resolution level. It reaches an excellent agreement at reconstructed resolution level $j = 4$. The results shed light on the application of wavelet multi-level method where the approximate WB solutions can be generated at a higher resolution levels from lower-level calculations.

Moreover, this approach can be applied in grid refinement. If we find the residual to be relatively large in a small subdomain, we can refine the mesh of the subdomain only using wavelet bases to improve accuracy and decrease computational cost. Thus, the properties of multiresolution analysis (MRA) can be used in an efficient manner to maintain different resolution levels for different regions of the solution domain.

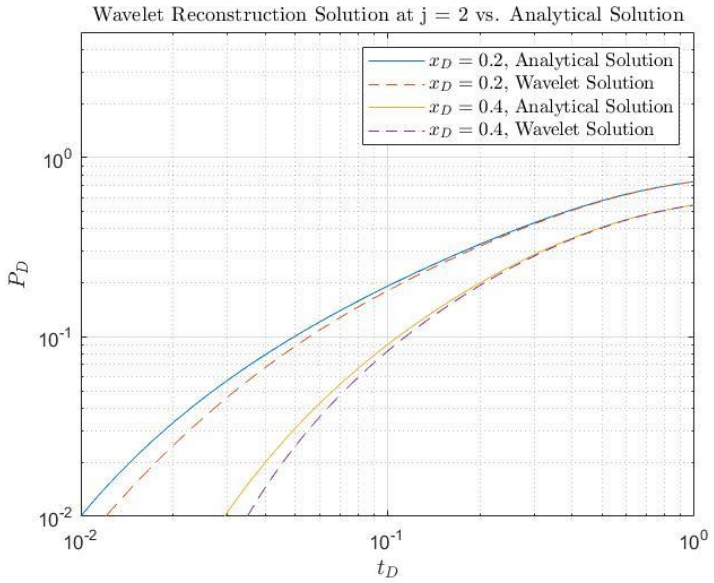

Figure 3.21 – Case 7: Comparison of (a) the analytical and (b) the WB reconstructed solution using cubic B-spline wavelet bases at j = 2: Reservoir pressure p_D as a function of t_D and x_D.

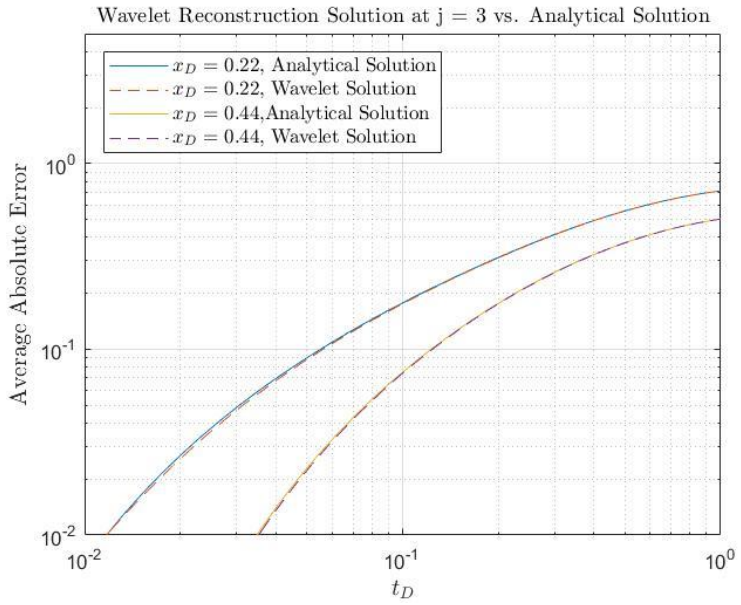

Figure 3.22 – Case 7: Comparison of (a) the analytical and (b) the WB reconstructed solution using cubic B-spline wavelet bases at j = 3: Reservoir pressure p_D as a function of t_D and x_D.

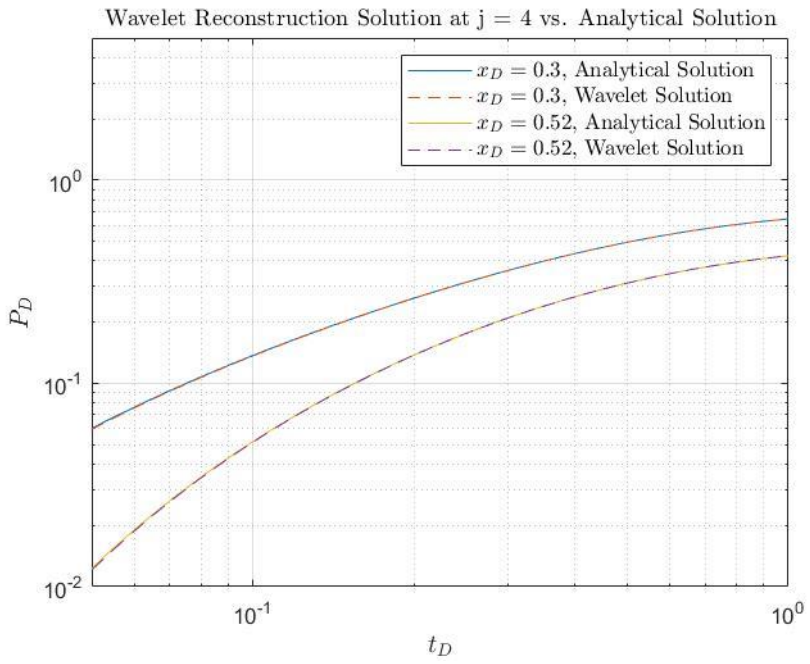

Figure 3.23 – Case 7: Comparison of (a) the analytical and (b) the WB reconstructed solution using cubic B-spline wavelet bases at j = 4: Reservoir pressure p_D as a function of t_D and x_D.

CHAPTER IV

SUMMARY, CONCLUSIONS, AND RECOMMENDATIONS FOR FUTURE WORK

4.1 Summary

The main goal of this study is to investigate the applicability and performance of wavelet-based (WB) numerical solutions in the solution of the linear and non-linear PDEs associated with the flow of fluids through porous and fractured (PF) media. In this approach, the wavelets are used to represent the spatial functions of the primary variables involved in the associated PDEs. The work was conducted using a MATLAB-based, purpose-built WB simulator, and the FTSim program (Wang, 2019) — a base version of the TOUGH + compositional non-isothermal numerical simulator (Moridis *et al.*, 1999, 2016) — also a conventional, fully implicit, Jacobian-based program that involves the Integral Finite-Difference scheme for space discretization for the analysis of fluid flow through PF media — was used for comparisons aimed to validate the WB simulator.

The study evaluated the performance of two typical wavelet bases: an orthogonal, and a biorthogonal one. The WB simulator (a) was verified through comparison to 1D flow problems with known analytical solutions, and (b) was validated by means of comparison of its results against the solutions to 2D and 3D problems obtained from the FTsim conventional simulator.

4.2 Conclusions

- Appropriate formulations of WB solutions using both Haar and B-spline basis functions have been developed and were shown to provide highly accurate solutions of flow and transport in problems of (a) 1D, 2D and 3D single phase, nearly incompressible (liquid) flow through porous media and (b) 1D two-phase flow under Buckley-Leverett conditions.
- The B-spline wavelet is highly flexible in a mathematical sense and can be seamlessly combined with FD-based discretization of the time domain to solve the PDEs of flow through porous media, while the Haar wavelets have some inherent difficulties in the treatment of the PDEs considered in this work and in the description/representation of the associated initial conditions.
- At the same resolution level, the WB method which uses B-spline wavelets yields consistently more accurate results than the methodology involving Haar wavelets. This is due to the different shapes of the wavelet bases, and the ability of the curvature in the B-spline wavelets to better conform to the shape of the solution surface.
- For the nonlinear Buckley-Leverett problem, as the resolution level increases, the accuracy of the solution increases. Also, as the B-spline order increases, the accuracy of the solution also increases. However, the B-spline order has a very limited impact on the accuracy of the solutions compared to the resolution level.
- The WB method based on the multiresolution property shows that higher-level approximate results can be obtained from the lower-level results and the reconstruction algorithm. This approach is particularly useful when the solution is

smooth in some subdomains and has abruptly changed in other subdomains. The grid refinement can be applied only on the specific subdomains.

- Because of the flexibility afforded by the process of construction and deconstruction of wavelets and their multi-resolution properties, WB methods have the potential to become powerful tools for solving coupled problems of multi-phase fluid flow (and possibly geomechanics) in 3D domains, thus providing integrated solutions to all aspects of problems of (a) multi-stage hydraulic fracturing and (b) coupled short- and long- term flow, production and geomechanics processes, including calculating fracture geometries, obtaining pressure changes between clusters and within each cluster, production rates and their evolution over time behavior, changes in the geometry and properties of the fractures and of the matrix, etc.

4.3 Future Recommendations for Future Work

- Exploit the innate multi-resolution property of wavelets for minimization of grid discretization and localized grid adaptation and refinement that allows resolution at any desired level, and use for the solution of complex multi-dimensional, intensely heterogeneous media with multiple fractures.
- Extend the proposed WB methods to multi-dimensional problems of multi-phase flow through complex porous and fractured media.
- Combine the wavelet basis functions with the finite element method to model rock deformation during and after hydraulic fracturing. The rate of convergence and the accuracy of this approach have been investigated by others and this work next stage of WB modeling should consider this problem.
- Combine wavelet basis functions with the boundary element method to perform fracture propagation analysis. This method is capable of meeting specific engineering needs and has the potential to significantly reduce the computational demands of the simulations by reducing the dimensionality of the problem.

REFERENCES

Abe, K., Koro, K., & Itami, K. (2001). An h-hierarchical Galerkin BEM using Haar wavelets. *Engineering Analysis with Boundary Elements, 25*(7), 581-591. doi:Doi 10.1016/S0955-7997(01)00015-7

Al-Qassab, M., & Nair, S. (2003). Wavelet-Galerkin method for free vibrations of elastic cable. *Journal of Engineering Mechanics, 129*(3), 350-357. doi:10.1061/(Asce)0733-9399(2003)129:3(350)

Al-Qassab, M., & Nair, S. (2004). Wavelet-Galerkin method for the free vibrations of an elastic cable carrying an attached mass. *Journal of Sound and Vibration, 270*(1-2), 191-206. doi:10.1016/S0022-460x(03)00490-5

Amaratunga, K., Williams, J. R., Qian, S., & Weiss, J. (1994). Wavelet-Galerkin Solutions for One-Dimensional Partial-Differential Equations. *International Journal for Numerical Methods in Engineering, 37*(16), 2703-2716. doi:DOI 10.1002/nme.1620371602

Barmada, S. (2007). Improving the performance of the boundary element method with time-dependent fundamental solutions by the use of a wavelet expansion in the time domain. *International Journal for Numerical Methods in Engineering, 71*(3), 363-378. doi:10.1002/nme.1946

Bindal, A., Khinast, J. G., & Ierapetritou, M. G. (2003). Adaptive multiscale solution of dynamical systems in chemical processes using wavelets. *Computers & Chemical Engineering, 27*(1), 131-142. doi:Pii S0098-1354(02)00165-5 Doi 10.1016/S0098-1354(02)00165-5

Blasingame, T.A. (1996). Lecture on *Linear Flow Solutions: Infinite and Finite-acting Reservoir Cases.* Personal Collection of T.A. Blasingame, Texas A&M University, College Station, Texas.

Bradley, J. N., Brislawn, C. M., & Hopper, T. (1993). The Fbi Wavelet Scalar Quantization Standard for Gray-Scale Fingerprint Image Compression. *Visual Information Processing Ii, 1961*, 293-304. doi:Doi 10.1117/12.150973

Burrus, C. S., Gopinath, R. A., & Guo, H. (1998). Introduction to wavelets and wavelet transforms: A primer. Upper Saddle River, N.J: Prentice Hall.

Bucher, H. F., Wrobel, L. C., Mansur, W. J., & Magluta, C. (2003). Fast solution of problems with multiple load cases by using wavelet-compressed boundary

element matrices. *Communications in Numerical Methods in Engineering, 19*(5), 387-399. doi:10.1002/cnm.598

Bucher, H. F., Wrobel, L. C., Mansur, W. J., & Magluta, C. (2004). On the block wavelet transform applied to the boundary element method. *Engineering Analysis with Boundary Elements, 28*(6), 571-581. doi:10.1016/j.enganabound.2003.10.002

Chen, X. F., Xiang, J. W., Li, B., & He, Z. J. (2010). A study of multiscale wavelet-based elements for adaptive finite element analysis. *Advances in Engineering Software, 41*(2), 196-205. doi:10.1016/j.advengsoft.2009.09.008

Chen, X. F., Yang, S. J., Ma, J. X., & He, Z. J. (2004). The construction of wavelet finite element and its application. *Finite Elements in Analysis and Design, 40*(5-6), 541-554. doi:10.1016/S0168-874x(03)00077-5

Chen, X. F., Yang, Z. B., Zhang, X. W., & He, Z. J. (2012). Modeling of wave propagation in one-dimension structures using B-spline wavelet on interval finite element. *Finite Elements in Analysis and Design, 51*, 1-9. doi:10.1016/j.finel.2011.10.007

Chen, Z. Y., Micchelli, C. A., & Xu, Y. S. (1997). The Petrov-Galerkin method for second kind integral equations .2. Multiwavelet schemes. *Advances in Computational Mathematics, 7*(3), 199-233. doi:Doi 10.1023/A:1018994802659

Chiavassa, G., & Liandrat, J. (2001). A fully adaptive wavel*et al.*gorithm for parabolic partial differential equations. *Applied Numerical Mathematics, 36*(2-3), 333-358. doi:Doi 10.1016/S0168-9274(00)00016-7

Chui, C. K., & Wang, J. (1991). A cardinal spline approach to wavelets. Proceedings of the American Mathematical Society, 113(3), 785-785. doi:10.1090/s0002-9939-1991-1077784-x

Chui, C. K., & Wang, J. Z. (1992a). A General Framework of Compactly Supported Splines and Wavelets. *Journal of Approximation Theory, 71*(3), 263-304. doi:Doi 10.1016/0021-9045(92)90120-D

Chui, C. K., & Wang, J. Z. (1992b). On Compactly Supported Spline Wavelets and a Duality Principle. *Transactions of the American Mathematical Society, 330*(2), 903-915. doi:Doi 10.2307/2153941

Chui, C., & Wang, J. (1993). An Analysis of Cardinal Spline-Wavelets. *Journal of Approximation Theory, 72*(1), 54-68. doi:10.1006/jath.1993.1006

Cruz, P., Mendes, A., & Magalhaes, F. D. (2001). Using wavelets for solving PDEs: an adaptive collocation method. *Chemical Engineering Science, 56*(10), 3305-3309. doi:Doi 10.1016/S0009-2509(00)00551-0

Dahmen, W., Kunoth, A., & Urban, K. (1996). A wavelet Galerkin method for the Stokes equations. *Computing, 56*(3), 259-301. doi:Doi 10.1007/Bf02238515

Daubechies, I. (1988). Orthonormal Bases of Compactly Supported Wavelets. *Communications on Pure and Applied Mathematics, 41*(7), 909-996. doi:DOI 10.1002/cpa.3160410705

Daubechies, I. (1990). The Wavelet Transform, Time-Frequency Localization and Signal Analysis. *Ieee Transactions on Information Theory, 36*(5), 961-1005. doi:Doi 10.1109/18.57199

Daubechies, I., & Lagarias, J. C. (1991). 2-Scale Difference-Equations .1. Existence and Global Regularity of Solutions. *Siam Journal on Mathematical Analysis, 22*(5), 1388-1410. doi:Doi 10.1137/0522089

Daubechies, I. (1992). *Ten lectures on wavelets*.

Dong, H. B., Chen, X. F., Li, B., Qi, K. Y., & He, Z. J. (2009). Rotor crack detection based on high-precision modal parameter identification method and wavelet finite element model. *Mechanical Systems and Signal Processing, 23*(3), 869-883. doi:10.1016/j.ymssp.2008.08.003

Eppler, K., & Harbrecht, H. (2003). Numerical solution of elliptic shape optimization problems using wavelet-based BEM. *Optimization Methods & Software, 18*(1), 105-123. doi:10.1080/1055678031000089629

Eppler, K., & Harbrecht, H. (2008). Wavelet-based boundary element methods for exterior electromagnetic shaping. *Engineering Analysis with Boundary Elements, 32*(8), 645-657. doi:10.1016/j.enganabound.2007.10.020

Gonzalez, P., Cabaleiro, J. C., & Pena, T. F. (2002). Parallel iterative solvers involving fast wavelet transforms for the solution of BEM systems. *Advances in Engineering Software, 33*(7-10), 417-426. doi:Pii S0965-9978(02)00047-9 Doi 10.1016/S0965-9978(02)00047-9

Goswami, J. C., Chan, A. K., & Chui, C. K. (1995). On Solving First-Kind Integral-Equations Using Wavelets on a Bounded Interval. *Ieee Transactions on Antennas and Propagation, 43*(6), 614-622. doi:Doi 10.1109/8.387178

Goupillaud, P., Grossmann, A., & Morlet, J. (1984). Cycle-Octave and Related Transforms in Seismic Signal Analysis. *Geoexploration, 23*(1), 85-102. doi:Doi 10.1016/0016-7142(84)90025-5

Haar, A. (1910). On the theory of orthogonal function systems (First announcement). *Mathematische Annalen, 69*, 331-371. doi:Doi 10.1007/Bf01456326

Han, J. G., Ren, W. X., & Huang, Y. (2006). A spline wavelet finite-element method in structural mechanics. *International Journal for Numerical Methods in Engineering, 66*(1), 166-190. doi:10.1002/nme.1551

Han, J. G., Ren, W. X., & Huang, Y. (2009). A spline wavelet finite element formulation of thin plate bending. *Engineering with Computers, 25*(4), 319-326. doi:10.1007/s00366-009-0124-7

Harbrecht, H., Paiva, F., Perez, C., & Schneider, R. (2002). Biorthogonal wavelet approximation for the coupling of FEM-BEM. *Numerische Mathematik, 92*(2), 325-356. doi:10.1007/s002110100283

He, Y. M., Chen, X. F., Xiang, J. W., & He, Z. J. (2007). Adaptive multiresolution finite element method based on second generation wavelets. *Finite Elements in Analysis and Design, 43*(6-7), 566-579. doi:10.1016/j.finel.2006.12.009

He, Y. M., Chen, X. F., Xiang, J. W., & He, Z. J. (2008). Multiresolution analysis for finite element method using interpolating wavelet and lifting scheme. *Communications in Numerical Methods in Engineering, 24*(11), 1045-1066. doi:10.1002/cnm.1011

Ho, S. L., & Yang, S. Y. (2001). Wavelet-Galerkin method for solving parabolic equations in finite domains. *Finite Elements in Analysis and Design, 37*(12), 1023-1037. doi:Doi 10.1016/S0168-874x(01)00040-3

Jin, J. M., Xue, P. X., Xu, Y. X., & Zhu, Y. L. (2006). Compactly supported non-tensor product form two-dimension wavelet finite element. *Applied Mathematics and Mechanics-English Edition, 27*(12), 1673-1686. doi:10.1007/s10483-006-1210-z

Kaneko, H., Noren, R. D., & Novaprateep, B. (2003). Wavelet applications to the Petrov-Galerkin method for Hammerstein equations. *Applied Numerical Mathematics, 45*(2-3), 255-273. doi:10.1016/S0168-9274(02)00173-3

Kim, Y. Y., Jang, G. W., & Kim, J. E. (2001). Multiscale wavelet-Galerkin method for meshless analysis of plane elasticity problems. *Computational Mechanics, Vols 1 and 2, Proceedings*, 959-964. Retrieved from <Go to ISI>://WOS:000177911800137

Ko, J., Kurdila, A. J., & Pilant, M. S. (1995). A Class of Finite-Element Methods Based on Orthonormal, Compactly Supported Wavelets. *Computational Mechanics, 16*(4), 235-244. Retrieved from <Go to ISI>://WOS:A1995RM54300003

Koro, K., & Abe, K. (2001). Non-orthogonal spline wavelets for boundary element analysis. *Engineering Analysis with Boundary Elements, 25*(3), 149-164. doi:Doi 10.1016/S0955-7997(01)00036-4

Koro, K., & Abe, K. (2003). A practical determination strategy of optimal threshold parameter for matrix compression in wavelet BEM. *International Journal for Numerical Methods in Engineering, 57*(2), 169-191. doi:DOI 10.1002/nme.666

Lepik, U. (2005). Numerical solution of differential equations using Haar wavelets. *Mathematics and Computers in Simulation, 68*(2), 127-143. doi:10.1016/j.matcom.2004.10.005

Lepik, U. (2007). Numerical solution of evolution equations by the Haar wavelet method. *Applied Mathematics and Computation, 185*(1), 695-704. doi:10.1016/j.amc.2006.07.077

Li, B., Cao, H. R., & He, Z. J. (2011). The construction of one-dimensional Daubechies wavelet-based finite elements for structural response analysis. *Journal of Vibroengineering, 13*(4), 729-738. Retrieved from <Go to ISI>://WOS:000299026100014

Li, B., & Chen, X. F. (2014). Wavelet-based numerical analysis: A review and classification. *Finite Elements in Analysis and Design, 81*, 14-31. doi:10.1016/j.finel.2013.11.001

Lu, D. F., Ohyoshi, T., & Miura, K. (1997). Treatment of boundary conditions in one-dimensional Wavelet-Galerkin method. *Jsme International Journal Series a-Solid Mechanics and Material Engineering, 40*(4), 382-388. doi:DOI 10.1299/jsmea.40.382

Ma, J. X., Xue, J. J., Yang, S. J., & He, Z. J. (2003). A study of the construction and application of a Daubechies wavelet-based beam element. *Finite Elements in Analysis and Design, 39*(10), 965-975. doi:Pii S0168-874x(02)00141-5 Doi 10.1016/S0168-874x(02)00141-5

Mallat, S. G. (1989). A Theory for Multiresolution Signal Decomposition - the Wavelet Representation. *Ieee Transactions on Pattern Analysis and Machine Intelligence, 11*(7), 674-693. doi:Doi 10.1109/34.192463

McWilliam, S., Knappett, D. J., & Fox, C. H. J. (2000). Numerical solution of the stationary FPK equation using Shannon wavelets. *Journal of Sound and Vibration, 232*(2), 405-430. doi:DOI 10.1006/jsvi.1999.2747

Mitra, M., & Gopalakrishnan, S. (2006a). Extraction of wave characteristics from wavelet-based spectral finite element formulation. *Mechanical Systems and Signal Processing, 20*(8), 2046-2079. doi:10.1016/j.ymssp.2005.01.003

Mitra, M., & Gopalakrishnan, S. (2006b). Wave propagation analysis in carbon nanotube embedded composite using wavelet based spectral finite elements. *Smart Materials and Structures, 15*(1), 104-122. doi:10.1088/0964-1726/15/1/039

Mitra, M., & Gopalakrishnan, S. (2006c). Wavelet based 2-D Spectral Finite Element formulation for wave propagation analysis in isotropic plates. *Cmes-Computer Modeling in Engineering & Sciences, 15*(1), 49-67. Retrieved from <Go to ISI>://WOS:000241043100005

Mitra, M., & Gopalakrishnan, S. (2006d). Wavelet based spectral finite element for analysis of coupled wave propagation in higher order composite beams. *Composite Structures, 73*(3), 263-277. doi:10.1016/j.compstruct.2005.01.038

Mitra, M., & Gopalakrishnan, S. (2006e). Wavelet based spectral finite element modelling and detection of de-lamination in composite beams. *Proceedings of the Royal Society a-Mathematical Physical and Engineering Sciences, 462*(2070), 1721-1740. doi:10.1098/rspa.2005.1653

Moridis, G. J., Anantraksakul, N., & Blasingame, T. A. (2021). Transformational-Decomposition-Method-Based Semianalytical Solutions of the 3D Problem of Oil Production from Shale Reservoirs. *Spe Journal, 26*(2), 780-811. doi:10.2118/199083-Pa

Moridis, G. J., Nikolaou, M., & You, Y. (1996). The Use of Wavelet Transforms in the Solution of Two-Phase Flow Problems. *Spe Journal, 1*(2), 169-177. doi:10.2118/29144-Pa

Moridis, G. J., & K. Pruess, User's Manual of the TOUGH+ Core Code: A General Purpose Simulator of Non-Isothermal Flow and Transport Through Porous and Fractured Media, Lawrence Berkeley National Laboratory report LBNL-6871E, February, 2016

Moridis, G. J., & Reddell, D. L. (1991). The Laplace Transform Finite-Difference Method for Simulation of Flow through Porous-Media. *Water Resources Research, 27*(8), 1873-1884. doi:Doi 10.1029/91wr01190

Moridis, G J, Wu, Y S, & Pruess, K. EOS9NT (1999): A TOUGH2 module for the simulation of water flow and solute/colloid transport in the subsurface. United States. https://doi.org/10.2172/765127

Morlet, J., Arens, G., Fourgeau, E., & Giard, D. (1982). Wave-Propagation and Sampling Theory .2. Sampling Theory and Complex Waves. *Geophysics, 47*(2), 222-236. doi:Doi 10.1190/1.1441329

Nakagoshi, S., & Noguchi, H. (2001). A modified wavelet Galerkin method for analysis of mindlin plates. *Jsme International Journal Series a-Solid Mechanics and Material Engineering, 44*(4), 610-615. doi:DOI 10.1299/jsmea.44.610

Nikolaou, M., & You, Y. (1994). Use of Wavelets for Numerical Solution of Differential Equations. In R. L. Motard & B. Joseph (Authors), *Wavelet applications in chemical engineering* (pp. 210-275). Boston: Kluwer Academic.

Oleary, D. P., & Widlund, O. (1979). Capacitance Matrix-Methods for the Helmholtz Equation on General 3-Dimensional Regions. *Mathematics of Computation, 33*(147), 849-879. doi:Doi 10.2307/2006065

Oruc, O., Bulut, F., & Esen, A. (2015). A Haar wavelet-finite difference hybrid method for the numerical solution of the modified Burgers' equation. *Journal of Mathematical Chemistry, 53*(7), 1592-1607. doi:10.1007/s10910-015-0507-5

Park, C., & Tsiotras, P. (2003a). Approximations to optimal feedback control using a successive wavelet collocation algorithm. *Proceedings of the 2003 American Control Conference, Vols 1-6*, 1950-1955. Retrieved from <Go to ISI>://WOS:000186706200330

Park, C., & Tsiotras, P. (2003b). Sub-optimal feedback control using a successive wavelet-Galerkin algorithm. *Proceedings of the 2003 American Control Conference, Vols 1-6*, 1926-1931. Retrieved from <Go to ISI>://WOS:000186706200326

Patton, R. D., & Marks, P. C. (1996). One-dimensional finite elements based on the Daubechies family of wavelets. *Aiaa Journal, 34*(8), 1696-1698. doi:Doi 10.2514/3.13291

Proskurowski, W., & Widlund, O. (1976). Numerical-Solution of Helmholtzs Equation by Capacitance Matrix-Method. *Mathematics of Computation, 30*(135), 433-468. doi:Doi 10.2307/2005318

Qian, S., & Weiss, J. (1993). Wavelets and the Numerical-Solution of Partial-Differential Equations. *Journal of Computational Physics, 106*(1), 155-175. doi:DOI 10.1006/jcph.1993.1100

Quraishi, S. M., & Sandeep, K. (2011). A second generation wavelet based finite elements on triangulations. *Computational Mechanics, 48*(2), 163-174. doi:10.1007/s00466-011-0586-5

Ravnik, J., Skerget, L., & Hribersek, M. (2004). The wavelet transform for BEM computational fluid dynamics. *Engineering Analysis with Boundary Elements, 28*(11), 1303-1314. doi:10.1016/j.enganabound.2004.05.002

Ravnik, J., Skerget, L., & Hribersek, M. (2006). Two-dimensional velocity-vorticity based LES for the solution of natural convection in a differentially heated enclosure by wavelet transform based BEM and FEM. *Engineering Analysis with Boundary Elements, 30*(8), 671-686. doi:10.1016/j.enganabound.2006.02.008

Ravnik, J., Skerget, L., Hribersek, M., & Zunic, Z. (2008). Numerical simulation of dilute particle laden flows by wavelet BEM-FEM. *Computer Methods in Applied Mechanics and Engineering, 197*(6-8), 789-805. doi:10.1016/j.cma.2007.09.007

Spasojevic, M., Schneider, R., & Levin, P. L. (1997). On the creation of sparse boundary element matrices for two dimensional electrostatics problems using the orthogonal Haar wavelet. *Ieee Transactions on Dielectrics and Electrical Insulation, 4*(3), 249-258. doi:Doi 10.1109/94.598281

Stehfest, H. (1970). Numerical Inversion of Laplace Transforms. *Communications of the Acm, 13*(1), 47-&. doi:Doi 10.1145/361953.361969

Sudarshan, R., D'Heedene, S., & Amaratunga, K. (2003). A multiresolution finite element method using second generation Hermite multiwavelets. *Computational Fluid and Solid Mechanics 2003, Vols 1 and 2, Proceedings*, 2135-2140. Retrieved from <Go to ISI>://WOS:000184938200521

Sweldens W., Schröder P. (2000) Building your own wavelets at home. In: Klees R., Haagmans R. (eds) Wavelets in the Geosciences. Lecture Notes in Earth Sciences, vol 90. Springer, Berlin, Heidelberg. https://doi.org/10.1007/BFb0011093

Tausch, J. (2003). Sparse BEM for potential theory and Stokes flow using variable order wavelets. *Computational Mechanics, 32*(4-6), 312-318. doi:10.1007/s00466-003-0488-2

Vasilyev, O. V., & Bowman, C. (2000). Second-generation wavelet collocation method for the solution of partial differential equations. *Journal of Computational Physics, 165*(2), 660-693. doi:DOI 10.1006/jcph.2000.6638

Vasilyev, O. V., & Kevlahan, N. K. R. (2005). An adaptive multilevel wavelet collocation method for elliptic problems. *Journal of Computational Physics, 206*(2), 412-431. doi:10.1016/j.jcp.2004.12.013

Vasilyev, O. V., & Paolucci, S. (1996). A dynamically adaptive multilevel wavelet collocation method for solving partial differential equations in a finite domain. *Journal of Computational Physics, 125*(2), 498-512. doi:DOI 10.1006/jcph.1996.0111

Venini, P., & Morana, P. (2001). An adaptive wavelet-Galerkin method for an elastic-plastic-damage constitutive model: 1D problem. *Computer Methods in Applied Mechanics and Engineering, 190*(42), 5619-5638. doi:Doi 10.1016/S0045-7825(01)00187-6

Wang, D., & Pan, J. (2004). A wavelet-Galerkin scheme for the phase field model of microstructural evolution of materials. *Computational Materials Science, 29*(2), 221-242. doi:10.1016/j.commatsci.2003.09.004

Wang, Q. Y. R. (2019) FTSim source code [Source Code]

Wang, Y. M., Chen, X. F., & He, Z. J. (2010). Adaptive Multiwavelet-Hierarchical Method for Multiscale Computation. *International Journal for Multiscale Computational Engineering, 8*(4), 397-409. Retrieved from <Go to ISI>://WOS:000283889000004

Wang, Y. M., Chen, X. F., & He, Z. J. (2011). An adaptive inverse iteration algorithm using interpolating multiwavelets for structural eigenvalue problems. *Mechanical Systems and Signal Processing, 25*(2), 591-600. doi:10.1016/j.ymssp.2010.08.007

Wang, Y. M., Chen, X. F., & He, Z. J. (2012). A second-generation wavelet-based finite element method for the solution of partial differential equations. *Applied Mathematics Letters, 25*(11), 1608-1613. doi:10.1016/j.aml.2012.01.021

Xiang, J. W., Chen, X. F., He, Z. J., & Zhang, Y. H. (2008). A new wavelet-based thin plate element using B-spline wavelet on the interval. *Computational Mechanics, 41*(2), 243-255. doi:10.1007/s00466-007-0182-x

Xiang, J. W., Chen, X. F., Li, B., He, Y. M., & He, Z. J. (2006). Identification of a crack in a beam based on the finite element method of a B-spline wavelet on the

interval. *Journal of Sound and Vibration, 296*(4-5), 1046-1052. doi:10.1016/j.jsv.2006.02.019

Xiang, J. W., Chen, X. F., Mo, Q. Y., & He, Z. J. (2007). Identification of crack in a rotor system based on wavelet finite element method. *Finite Elements in Analysis and Design, 43*(14), 1068-1081. doi:10.1016/j.finel.2007.07.001

Xiang, J. W., & Liang, M. (2012a). A two-step approach to multi-damage detection for plate structures. *Engineering Fracture Mechanics, 91*, 73-86. doi:10.1016/j.engfracmech.2012.04.028

Xiang, J. W., & Liang, M. (2012b). Wavelet-Based Detection of Beam Cracks Using Modal Shape and Frequency Measurements. *Computer-Aided Civil and Infrastructure Engineering, 27*(6), 439-454. doi:10.1111/j.1467-8667.2012.00760.x

Xiang, J. W., Matsumoto, T., Long, J. Q., & Ma, G. (2013). Identification of damage locations based on operating deflection shape. *Nondestructive Testing and Evaluation, 28*(2), 166-180. doi:10.1080/10589759.2012.716437

Xiang, J. W., Matsumoto, T., Long, J. Q., Wang, Y. X., & Jiang, Z. S. (2012). A simple method to detect cracks in beam-like structures. *Smart Structures and Systems, 9*(4), 335-353. doi:DOI 10.12989/sss.2012.9.4.335

Xiang, J. W., Matsumoto, T., Wang, Y. X., & Jiang, Z. S. (2011). A Hybrid of Interval Wavelets and Wavelet Finite Element Model for Damage Detection in Structures. *Cmes-Computer Modeling in Engineering & Sciences, 81*(3-4), 269-294. Retrieved from <Go to ISI>://WOS:000301207800003

Xiang, J. W., Matsumoto, T., Wang, Y. X., & Jiang, Z. S. (2013). Detect damages in conical shells using curvature mode shape and wavelet finite element method. *International Journal of Mechanical Sciences, 66*, 83-93. doi:10.1016/j.ijmecsci.2012.10.010

Xiao, J. X., & Tausch, J. (2010). A fast wavelet-multipole method for direct BEM. *Engineering Analysis with Boundary Elements, 34*(7), 673-679. doi:10.1016/j.enganabound.2010.01.009

Xiao, J. Y., Tausch, J., Cao, Y. C., & Wen, L. H. (2009). Combined equivalent charge formulations and fast wavelet Galerkin BEM for 3-D electrostatic analysis. *International Journal for Numerical Methods in Engineering, 79*(6), 753-772. doi:10.1002/nme.2598

Xiao, J. Y., Tausch, J., & Hu, Y. C. (2009). A-posteriori compression of wavelet-BEM matrices. *Computational Mechanics, 44*(5), 705-715. doi:10.1007/s00466-009-0403-6

Xiao, J. Y., Wen, L. H., & Tausch, J. (2009). On fast matrix-vector multiplication in wavelet Galerkin BEM. *Engineering Analysis with Boundary Elements, 33*(2), 159-167. doi:10.1016/j.enganabound.2008.05.006

Xiao, J. Y., Wen, L. H., & Zhang, D. (2007). A wavelet-integration-free periodic wavelet Galerkin BEM for 2D potential problems. *Engineering Computations, 24*(3-4), 306-318. doi:10.1108/02644400710748661

Xiao, J. Y., & Ye, W. J. (2011). Wavelet BEM for large-scale Stokes flows based on the direct integral formulation. *International Journal for Numerical Methods in Engineering, 88*(7), 693-714. doi:10.1002/nme.3198

Yang, S. Y., Ni, G. Z., Qian, J. G., & Li, R. L. (1998). Wavelet-Galerkin method for computations of electromagnetic fields. *Ieee Transactions on Magnetics, 34*(5), 2493-2496. doi:Doi 10.1109/20.717574

Yang, Z. B., Chen, X. F., Li, B., He, Z. J., & Miao, H. H. (2012). Vibration Analysis of Curved Shell using B-spline Wavelet on the Interval (BSWI) Finite Elements Method and General Shell Theory. *Cmes-Computer Modeling in Engineering & Sciences, 85*(2), 129-155. Retrieved from <Go to ISI>://WOS:000307601400002

Yang, Z. B., Chen, X. F., Zhang, X. W., & He, Z. J. (2013). Free vibration and buckling analysis of plates using B-spline wavelet on the interval Mindlin element. *Applied Mathematical Modelling, 37*(5), 3449-3466. doi:10.1016/j.apm.2012.07.055

Zhang, T. H., Tian, Y. C., & Tade, M. O. (2008). Wavelet-based collocation method for stiff systems in process engineering. *Journal of Mathematical Chemistry, 44*(2), 501-513. doi:10.1007/s10910-007-9324-9

Zhong, Y. T., & Xiang, J. W. (2011). Construction of Wavelet-Based Elements for Static and Stability Analysis of Elastic Problems. *Acta Mechanica Solida Sinica, 24*(4), 355-364. Retrieved from <Go to ISI>://WOS:000295296900007

Zhou, Y. H., & Zhou, J. (2008). A modified wavelet approximation of deflections for solving PDEs of beams and square thin plates. *Finite Elements in Analysis and Design, 44*(12-13), 773-783. doi:10.1016/j.finel.2008.05.001